Nano-Structures & Nano-Objects 26 (2021) 100728

Contents lists available at ScienceDirect

Nano-Structures & Nano-Objects

journal homepage: www.elsevier.com/locate/nanoso

Review on functional bi-component nanocomposites based on hard/soft ferrites: Structural, magnetic, electrical and microwave absorption properties

M.A. Almessiere [a,*], Y. Slimani [a,*], A.V. Trukhanov [b,c,**], A. Sadaqat [d], A. Demir Korkmaz [e], N.A. Algarou [a,f], H. Aydın [g], A. Baykal [h], Muhammet S. Toprak [i]

[a] Department of Biophysics, Institute for Research and Medical Consultations (IRMC), Imam Abdulrahman Bin Faisal University, P.O. Box 1982, 31441 Dammam, Saudi Arabia
[b] Scientific-Practical Materials Research Centre of National Academy of Sciences of Belarus, 220072 Minsk, Belarus
[c] South Ural State University, 454080 Chelyabinsk, Russia
[d] Mechanical and Energy Engineering Department, College of Engineering, Imam Abdulrahman Bin Faisal University, P.O. Box 1982, 31441 Dammam, Saudi Arabia
[e] Department of Chemistry, Istanbul Medeniyet University, 34700 Uskudar-Istanbul, Turkey
[f] Department of Physics, College of Science, Imam Abdulrahman Bin Faisal University, P.O. Box 1982, 31441 Dammam, Saudi Arabia
[g] Faculty of Engineering, Department of Chemistry, İstanbul University-Cerrahpaşa, 34320, Avcılar/İstanbul, Turkey
[h] Department of Nanomedicine Research, Institute for Research and Medical Consultations (IRMC), Imam Abdulrahman Bin Faisal University, P.O. Box 1982, 31441 Dammam, Saudi Arabia
[i] Department of Applied Physics, KTH Royal Institute of Technology, SE 10691 Stockholm, Sweden

ARTICLE INFO

Article history:
Received 3 February 2021
Received in revised form 12 March 2021
Accepted 19 March 2021

Keywords:
Hard/soft ferrites
Synthesis
Microstructure
Electrical and magnetic properties
Microwave absorber

ABSTRACT

Bi-component hard (H) (hexaferrite) and soft (S) (spinel) ferrites nanocomposites are gaining interest scientifically and technically, not only for combining the high magnetization of spinel ferrite nanomaterials and the high coercivity of hexaferrite magnetic nanomaterials but also for the outstanding exchange-coupling behavior among hard and soft magnetic phase. The improved magnetic features lead to produce a new nanocomposite with higher microwave absorption capacity in comparison with ferrites with a single absorption mechanism. Exchange-coupled effect has a potential application based on microwave absorption, recording media, permanent magnets, biomedical and other applications. Intensive studies have been conducted on this topic to produce hard/soft (H/S) ferrite nanocomposites with establishment of exchange coupled effect between the two phases. Preparation methods, microstructure, magnetics features, microwave and dielectric properties, and applications are elaborated. Consequently, a comprehensive effort has been made to contain an original reference investigating in detail the precise outcomes of the published papers.

Contents

* Corresponding authors at: Department of Biophysics, Institute for Research and Medical Consultations (IRMC), Imam Abdulrahman Bin Faisal University, P.O. Box 1982, 31441 Dammam, Saudi Arabia.
** Corresponding author at: Scientific-Practical Materials Research Centre of National Academy of Sciences of Belarus, 220072 Minsk, Belarus.
E-mail addresses: malmessiere@iau.edu.sa (M.A. Almessiere), yaslimani@iau.edu.sa (Y. Slimani), truhanov86@mail.ru (A.V. Trukhanov).

https://doi.org/10.1016/j.nanoso.2021.100728
2352-507X/

1. Introduction

With the recent advancements in various fields of technology, there has been a search for multi-functional nanocomposites made of different phases [1]. Magnetic nanoparticles (MNP) have been employed in numerous fields ranging from biomedical applications to environmental studies (catalysis, adsorption, etc.) and from radio communication to electronics (radar absorbing materials, electrodes for batteries, magnetic recording heads, etc.) [2–18]. The developments in synthetic chemistry allows us not only to synthesize MNP but also to engineer them with the desired properties. Combining materials with different characteristics to obtain a new functional material (core–shell, bilayer, etc.) is a key method to achieve this goal. hard hexagonal and soft spinel ferrites are well reputable during the past years [19–22]. Certainly, these magnets nanocrystalline have established attractively electromagnetic features that can processed the challenges of today's electronic devices [23,24]. Soft/hard ferrite composites highly appreciate because of their unique magnetization, coercivity, microwave absorption and electro-magnetic properties [25–27]. Moreover, they have certain features such as high magnetic anisotropy (K), high electrical resistivity, low initial susceptibility in addition to the maximum energy product (BH_{max}, is the energy density that a hard ferrite can store with low magnetic anisotropy) [28]. So, the magnetic features can be tuned via the exchange-coupling among soft and hard phases to fabricate the nanocomposite with the desired properties [29–32]. Recently, these types of materials have been paid substantial consideration due to its excellent the magnetic properties. It is confirmed that magnetic interaction, microstructure, composition, and grain size are highly affected the exchange-coupling of soft and hard ferrites [33,34]. Many researchers have been published the magnetic and structural properties have been improved by suitable mass ratio, calcination, and exchange-coupling of soft and hard ferrites [35–38].

Most of the magnetic materials having less valve of saturation of magnetization (M_s) and high coercivity (H_c), has become a challenging task to reach high M_s and H_c at the same time [39]. However, spinel soft and hard ferrite composites are favorable for progressed permanent magnetic materials, owing to their high Curie temperature, outstanding corrosion resistance and high electrical resistivity etc. [40]. Soft spinel ferrite having a low anisotropic also suitable for microwave application [41]. Conversely, hard hexaferrite such as $BaFe_{12}O_{19}$ or $SrFe_{12}O_{19}$ has high ferromagnetic resonance frequency (35 GHz) and high magneto-crystalline anisotropy that is suitable up to W- band [42]. Accordingly, combination low anisotropic soft ferrite and high anisotropic hard ferrite frequently utilized for different microwave device applications [43,44]. Radar absorbing materials (RAM) have an outstanding microwave absorbing material because of its high range between 8.2–12.4 GHz [45]. Nevertheless, large absorption peak, wide working frequency range and thin absorption layer cannot accomplish by using a single material as an ideal radar absorber [46,47]. Nanocomposites offer to create a consolidated system containing between soft and hard ferrite phases, which characteristics are exclusive and complimentary [48]. The magneto-dielectric composites have high permeability and high permittivity nature due to the exchange-coupling. However, some composites used in scarcely investigation owing to their high frequencies range between 12–18 GHz [49,50].

In the following paragraphs, we first introduce the structural features of the constituent ferrites in the bi-component H/S and S/H nanocomposites followed by the experimental techniques to produce such systems and their impact on the products including but not limited to crystallite size, grain shapes and microstructural challenges presented. Finally, we will discuss about the changes arising in the magnetic behavior after developing the nanocomposites of hard and soft ferrites in the subsequent paragraphs. We will also present a review on the novel dielectric characteristics of H/S and S/H bi-component nanocomposites and their exchange coupled effects in addition to the microwave absorption characteristics.

2. Structural features of ferrites

Ferrites, ferrimagnetic oxides of ferric oxide and metal oxides, are a class of compounds with different subclasses. We can categorize ferrites based on their magnetic behavior and crystal structures. These are spinel ferrites (AFe_2O_4, where A is usually a transition metal such as Fe, Mn, Zn, Co, Co, Ni, etc.), garnet ferrites ($RE_3Fe_5O_{12}$, where RE stands for rare earth cations), hexaferrites or hexagonal ferrites (the most popular type being M-type with the formula $MFe_{12}O_{19}$ where M is usually Ba^{2+} or Sr^{2+}) and orthoferrites ($MFeO_3$). In our review, we will focus on the nanocomposites of spinel ferrites and M-type hexaferrites.

2.1. Spinel ferrites

The formula for spinel crystal structure is AB_2O_4 (A^{2+} and B^{3+} metal ions). In spinel ferrites, B is replaced with Fe^{3+}, thus making the formula AFe_2O_4. The oxygen ions, with their large size (radius is ~0.13 nm), are packed tightly resulting in a face-centered cubic (*fcc*) rearrangement and the smaller metal atoms are packed in the remaining spaces between them which are the tetrahedral (**A**) (T_d) and the octahedral (**B**) (O_h) sites [51] (Fig. 1). M^{2+} and Fe^{3+}

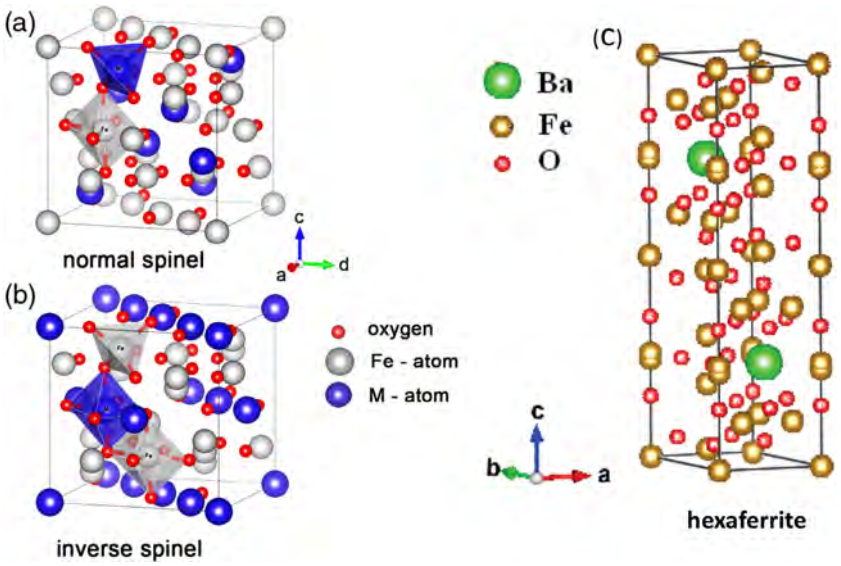

Fig. 1. Crystal structures of spinel ferrites (a) normal spinel, (b) inverse spinel and hexaferrite [23].

ions can occupy either **A** or **B** interstitial sites in the spinel ferrites based on their type [52]. Spinel compounds can be classified as normal, inverse, and mixed based on the distribution of cations over the crystallographic sites within crystal (Fig. 1).

In a spinel ferrite, there are eight formula units or octants, and $8 \times 7 = 56$ atoms composed of 32 anions and 24 cations, per unit cell. Although there are 96 interstices between the anions in the spinel unit cell, cations reside only in the 24 of these interstices: 8 reside in the tetrahedral interstices out of 64 T_d interstices and the 16 cations remaining occupy half of the 32 O_h interstices [53] therefore the actual formula becomes $A_8B_{16}O_{32}$. The lattice parameter '*a*' is equal to the periodicity related to the octahedrally coordinated cation sublattices as well as the repeat unit of the diamond cubic sublattice formed by the tetrahedrally coordinated cations [53].

In normal spinel, $A_{T_d}(B_2)_{O_h}O_4$ all the trivalent ions (B^{3+}) exist in O_h sites whereas the divalent cations (A^{2+}) be located in T_d sites . $ZnFe_2O_4$ is a common spinel ferrite. Some oxides of aluminum and chromium (MAl_2O_4 and MCr_2O_4 where M can be Mg^{2+}, Fe^{2+}, Co^{2+}, and Zn^{2+}) also adopt the normal spinel structure [54].

In inverse spinel ferrites, half of the tetrahedral positions are filled with the trivalent cations. The rest of the T_d interstices is composed of the divalent cations and the O_h sites are filled with A^{3+}. The site occupancy of the inverse spinel can be shown as $B_{T_d}(AB)_{O_h}O_4$ which is present in most of the ferrites of the first transition metal series such as maghemite, magnetite, $CoFe_2O_4$, and $CuFe_2O_4$ [55].

A spinel ferrite can display ferromagnetic, antiferromagnetic, spin (cluster) glass, and paramagnetic behavior depending on the cations on the A and B sites. The distribution of cations between O_h and T_d sites determines the strange properties of them. So, the control of cation distribution provides a means to tailor their properties [56–58]. That is why various cation types can be introduced in A- and B-sites to develop the magnetic characteristics of spinel ferrites and hence obtain H/S nanocomposites with novel compositions and features.

2.2. Hexaferrites

Barium hexaferrite was the first synthetic hexaferrite produced and strontium hexaferrites were discovered by a team of scientists lead by Snoek in Philips Laboratories in Eindhoven, Netherlands in the 1950s. For instance, Wijn and Braun, also in the Philips team published a report on producing other hexagonal materials based on the BaM ($BaO{\cdot}Fe_2O_3$) such as $BaFe_{18}O_{27}$ which contained both Fe^{2+} and Fe^{3+} ions [59–61]. This was followed by the synthesis of novel related compounds upon heating BaO–Fe_2O_3–MeO (Me: a small cation with +2 charge) ternary system between 1200 °C and 1400 °C by the same team. Finally, these were reported in a book titled "Ferrites" in 1959 by Smit and Wijn [62]. It was facile to produce the M-type barium hexaferrite which had a high coercivity (160 to 255 kA/m), thus called magnetically hard also had distinguishable features such as high electrical resistivity (10^8 Ω.cm) and high magnetic uniaxial anisotropy alongside the c-axis [62]. The BaM has a magnetic hardness of 5.9 GPa and 6.0 GPa theoretically and practically, respectively [63–68]; a maximum density of 5.296 g/cm^3 and a molar mass (M.M.) of 1112 g/mol. Strontium hexaferrite (SrM) is also another hexaferrite with a formula of $SrFe_{12}O_{19}$ and has a maximum density of 5.101 g/cm^3 and a M.M. of 1062 g/mol along with other similar physical features with BaM. In lead hexaferrite (PbM), the divalent barium is replaced with Pb^{2+} which has a high molecular mass compared to barium, and thus the M.M. of PbM is 1181 g/mol while its density is 5.708 g/cm^3 [69].

The crystal structure of M-type hexaferrites has stacking sequences alternating between R- and S-blocks which lie along the c axis as shown in Fig. 1. The R-block has three layers, and the S-block has two layers. The S-block is a spinel and hence has the formula $Me_2Fe_4O_8$, and when Me is the iron ion it is Fe_6O_8. In the S-block there are six trivalent iron ions with two layers of 4 oxygen atoms and between each layer, there are 3 metal atoms, making it a 6 total. There are two T_d sites in which the cation is surrounded by 4 O^{2-} ions and four O_h sites in which the cation is encircled by 6 O^{2-} ions [70–73].

The R-block has hexagonally packed three layers and each layer consists of 4 oxygen ions. However, in the middle layer of the oxygen atoms are replaced with Ba^{2+}, which has a similar size with that of the oxygen and thus the formula becomes $BaFe_6O_{11}$. This middle layer is equivalent to M_5 unit when the bottom and top layers are eliminated. Ba ions lead to asymmetry in parts of the structure including cations and hence five O_h sites are formed while the large Ba ion pushes the T_d sites to O_h sites. Finally, there is a trigonal bipyramidal site where 5 O^{2-} ions enclose the cation [64].

In a typical M-type hexaferrite unit cell, there are R- and S-blocks stacked along the hexagonal axis. Their stacking order is RSR*S* where S and S* have 6 Fe^{3+} ions while R and R* blocks have 6 Fe^{3+} ions, making it 12 Fe^{3+} ions. The unit cell of M-type hexaferrite is $P6_3/mmc$ which has a total of five crystallographic sites, namely tetrahedral ($4f_1$), octahedral ($12k$, $4f_2$, and $2a$), and hexahedral (trigonal bipyramidal) ($2b$) sites [74]. The spin of $4f_1$ and $4f_2$ sites which contain Fe^{3+} ions (8 ions/unit cell) is downwards and the spin of Fe^{3+} ions (16 ions/unit cell) at the $12k$, $2a$, and $2b$ sites is upwards [75]. Every S-block possesses 4 O_h, 2 opposite T_d magnetic moments and there is a total of 2 magnetic moments. The R-block possesses five-coordinate trigonal bipyramidal sites, which are aligned with 3 of 5 O_h moments because of the distortion, making the net moment 2. At absolute zero, there is a magnetic moment of 5 μB in Fe^{3+} ions. Therefore, there is a total of $8 \times 5 = 40$ μB magnetic moments in BaM. The large uniaxial magneto-crystalline anisotropy of BaM can be tuned by the substitution of especially trivalent iron ions with different cations.

2.3. Hard/soft nanocomposites

H/S ferrite nanoparticles have similar properties in both core/shell formation and bilayer formation. The soft phase usually has a large saturation magnetization (M_s) and low anisotropy constant, resulting in a small coercivity (H_c). The hard phase carries out a mild level M_s, large K, and high H_c. We can state that the general trend in their behavior is somewhat between soft and hard phases. The soft layer dimensions in films and the soft phase thickness (t_{soft}) in thin films were shown to affect the switching behavior of magnetization.

3. Exchange-coupling

The intrinsic microstructural characteristics as well as magnetic features determine the magnetic fate of the magnetic materials. We can add grain boundary, size, and many other characteristics as well [75]. The term exchange coupled composite leads back to 1990s when they were defined by Kneller and Hawing [76]. This system was composed of two phases, which were mutually coupled. H/S magnetic oxide-based nano-sized powders and bilayer thin films were of interest. When the exchange-coupling is succeeded, coherent spin rotations produce a smooth demagnetization behavior and hence a smooth hysteresis curve. In non-coupled systems, however, individual soft and hard spin switching results in a stepped hysteresis curve. Several factors are affecting the formation of exchange-coupling. For example, in films, the magnetization switch is known to depend on the film thickness in thin films.

The exchange-coupling also be contingent on the exchange stiffness of the interface and magnetic interaction, grain size, and the exchange distance correlated with the microstructure according to theoretical studies [77]. Therefore, there are some requirements for H/S systems to successfully occur with exchange-coupling of the soft and hard phases. These are: (1) there must be an intimate contact between the phases such as bilayer, particle composites, core–shell, etc. (2) twice the width of the domain wall of the hard phase ($2\delta_H$) should not be exceeded by the soft phase's particle size in a composite film [78]. Below this critical thickness, the soft phase is strictly coupled to the hard phase and both phases form a rectangular hysteresis curve by reversing simultaneously at the nucleation field (H_N). Above this thickness, the soft phase reverses at the nucleation field while the hard phase does not do so. When the exchange field of the soft phase is exceeded; just like in a magnetic domain wall, the soft phase's spins start a continuous rotation whose angle increases with as the distance from the hard phase is increased, causing a twist of the magnetization in this phase a magnetic reversal [75]. When the reverse field is detached, the soft phase shows an alignment with the hard phase, and thus a reversible magnetization curve is obtained. This process is usually called as the exchange-spring process. On the other hand, different factors should be considered while dealing with core–shell H/S nanocomposites. For instance, some studies have found the nucleation field (H_N) depends on the shell thickness and such parameters [79]. In addition, the magnetic characteristics are affected by the structure of the core/shell composite, i.e. H/S or S/H. In H/S core/shell composites, as the amount of soft layer increases, the H_C drops and the M_S increases [80–82]. Oppositely, in S/H core/shell systems, as the hard layers are grown, H_C rises and M_S drops [83–85]. In some systems, on the other hand, HC varies with the volume ratio of H/S if there is a small difference of M_S between the phases [86–88].

In the literature, we can see that there have been many attempts to produce exchange-coupled nanocomposites. As stated before, we focus on the H/S or S/H ferrite nanocomposites composed of hexaferrites and cubic spinel ferrites with different compositions for various purposes. The soft/hard (S/H) ferrite composites were synthesized by numerous researchers in the search for the perfect S/H ferrite in exchange-coupling. For example, the effect of mass ratio in $Ni_{0.5}Zn_{0.5}Fe_2O_4/SrFe_{12}O_{19}$ was investigated, and it was found to display great magnetic traits and good microwave absorption ((Reflection Loss $\leq$ 10 dB) enhanced to 6.4 to 9.3 GHz from 2.9 GHz) [77]. Other groups reported $NiFe_2O_4/BaFe_{12}O_{19}$. The H/S ferrite nanocomposites were investigated for distinct characteristics and/or applications. For instance, some groups evaluated the exchange-coupling of nanocomposites (NC). However, the complex microstructural behavior of oxide NC poses a challenge to tune their characteristics. So, there are more reports on bulk H/S ferrites when compared to their nano-sized counterparts [19]. Some of these included $BaFe_{12}O_{19}/Ni_{0.5}Zn_{0.5}Fe_2O_4$ NC with different weight ratios, $SrFe_{12}O_{19}/\gamma$-Fe_2O_3 nanocomposites, and $SrFe_{12}O_{19}/NiFe_2O_4$ [89–91]. On the other hand, the H/S nanocomposite studies are mostly on M-type hexaferrites with cubic spinel ferrites including $BaFe_{12}O_{19}/Ni_{0.8}Zn_{0.2}Fe_2O_4$ [92], $BaFe_{12}O_{19}/Y_3Fe_5O_{12}$ [93], $SrFe_{12}O_{19}/NiFe_2O_4/ZnFe_2O_4$ [91], $SrFe_{10}Al_2O_{19}/Co_{0.8}Ni_{0.2}Fe_2O_4$ [94], and $SrFe_{12-x}V_xO_{19}/(Ni_{0.5}Mn_{0.5}Fe_2O_4)_y$ [95].

4. Exchange bias

The loop shifts in the field axis part of the magnetic hysteresis curve of the exchange-coupled H/S ferrites is known as the "exchange bias". The term was initially described by Meiklejohn and Bean in 1956 [96] and has been a topic of interest since then. In the exchange-coupled magnetic systems, the core and the shell or the H/S phases display magnetic characteristics (ferromagnetic (FM), antiferromagnetic (AFM) or ferrimagnetic (FiM)). When an H/S nanocomposite core/shell or bilayer in the form of a ferromagnetic (FM)-antiferromagnetic (AFM) composition is cooled down below the Néel temperature, due to the AFM phase, an asymmetric shift in the field axis occurs which is known as the exchange bias [97]. There are different influences on the shift of the loop's magnitude (H_{EB}). Some of these are the interfacial complicated structure of the spins, and any other unbalanced interface moments, properties of the existing layers such AFM-FM making up the H/S nanocomposite, interface roughness, etc. When the hysteresis shift is parallel with the cooling field (H_{CF}), it is called as the positive exchange bias (PEB) and when it is on the reverse side of the H_{CF}, it is called as the negative exchange bias (NEB) [98]. The exchange-coupling due to the AFM is usually held responsible for the hardly experienced PEB. The magnitude of the AFM and its sign also is HCF dependent. Some systems displaying PEB are $Ni_{81}Fe_{19}/Ir_{20}Mn_{80}$ bilayers because of the FM/AFM

interface magnetic disorder due to the magnetic training effect (TE) and thin films of FeF_2/Fe bilayer [98]. On the other hand, the interface coupling of AFM and FM phases existing together in $Cu_{1-x}Mn_x$/Co at low temperatures resulted in NEB [99]. Rana et al. prepared a $La_{0.3}Sr_{0.7}FeO_3/SrRuO_3$ bilayer on a disordered interface of a mosaic $SrTiO_3$ substrate and observed a PEB at a low cooling field (about one Tesla) which shifted to NEB at a high cooling field (7 T) which meant the giant vertical shift and positive exchange bias in magnetic oxides could be tuned by applying different factors [97].

5. Purpose of the review

The main goal of this study is to present an overview about the correlation between microstructure, magnetic, microwave, dielectric properties, and exchange-coupled effect of Hard/soft (spinel) ferrites nanocomposites. Based on our information, this is the first review presented on the status and recent studies about functional bi-component nanocomposites based on H/S ferrites. H/S ferrites have an exceptional niche of nanocomposites due to the huge attention of the scientific community. Accordingly, this study will introduce the challenges of exchange-coupling behavior due to the sophisticated fabrication methods, microstructural difficulties, grain shapes and crystallite size that are hard to compute and regulate. The review presents the latest accomplishment of H/S ferrites nanocomposites in microwave absorption.

6. Synthesis Methods of H/S nanocomposites

6.1. One-pot sol–gel auto-combustion process

One-pot sol–gel auto-combustion process is the combination of chemical sol–gel and following combustion routes. The desired metal salts having an aqueous solution, through a sol–gel process obtain organic fuel forms as a gel. Subsequently, fluffy, yielding, and voluminous products with large surface area achieved by ignition to combust the gel as seen in Fig. 2. Torkian et al. [94] have used this method to prepare the $SrFe_{10}Al_2O_{19}/Co_{0.8}Ni_{0.2}Fe_2O_4$ H/S nanocomposite. In a typical procedure, de-ionized water was used to dissolve stoichiometric amounts of metal nitrates at 60 °C, by the addition of citric acid. Subsequently, an accomplishment of the procedure, the solutions were cooled down to room temperature. It has been noticed that synthesis temperature was reduced, evaporation was minimized, and high purity of final products was achieved. This is a very important technique for synthesizing exchange-coupled magnetic materials.

Numerous researchers have reported on the synthesis of H/S ferrites NCs $Sr_{0.3}Ba_{0.4}Pb_{0.3}Fe_{12}O_{19}/(CuFe_2O_4)_x$ [100], $SrTb_{0.01}Tm_{0.01}Fe_{11.98}O_{19}/CoFe_2O_4$ [101], $SrFe_{10}Al_2O_{19}/Co_{0.8}Ni_{0.2}Fe_2O_4$ [94], and studied the structural, magnetic and microwave properties via one-pot sol–gel process. Almessiere et al. [100] synthesized the H/S $Sr_{0.3}Ba_{0.4}Pb_{0.3}Fe_{12}O_{19}/(CuFe_2O_4)_x$ NCs by using one-pot citrate sol–gel route using citric acid and metal nitrates as precursors. Suitable amounts of metal nitrates and de-ionized water were stirred on a hotplate at 80 °C until a clear solution was obtained, during stirring, a citric acid solution was slowly added into the resulting mixture. Throughout evaporation, a viscous brown gel was obtained. The desired nanocomposite powder achieved by preheated to 500 °C for 1 h and then calcined at 1100 °C for 2 h. Additionally, due to the exchange-coupling interaction suitable values of squareness ratio, remanent (M_r) and saturation (M_s) magnetizations and coercivity (H_c) were found for the $Sr_{0.3}Ba_{0.4}Pb_{0.3}Fe_{12}O_{19}/CuFe_2O_4$ NCs. Algarou et al. [102] introduced $SrCo_{0.02}Zr_{0.02}Fe_{11.96}O_{19}/MFe_2O_4$ (M = Mn, Zn, Co, Ni, and Cu) H/S NCs via one-pot sol–gel combustion approach. The solutions mixed with the addition of citric acid by stirring at 95 °C. To maintain the pH at 7, alkaline solution was added, and the mixture was heated at 160 °C for 45 min up to 350 °C. A black powder was obtained, that was calcined at 950 °C for 6 h, finally resulting in hard and soft ferrites' structure. Afshar et al. [103] fabricated the $SrFe_{12}O_{19}$ and $Ni_{0.6}Zn_{0.4}Fe_2O_4$ ferrites by single-pot approach. They studied phase, microstructure, and magnetic properties as a function of the amount of NiZn ferrite. It has been observed that spinel NiZn ferrites display a high permeability, low anisotropy field along with microwave absorption.

6.2. Ball milling

Ball milling (BM) is a mechanical method extensively used to grind powders into fine particles and blend materials. It is a cost-effective technique and widely used in industrial applications. BM has been used according to the application. It usually contains a hollow cylindrical shell rotating around its axis, this shell is partially filled with balls having different materials such as ceramic, steel, and stainless steel. It depends on the released energy from attrition and impact between the balls that accomplish grinding or milling and the powder as revealed in Fig. 2. The main advantages of this method consist of ease of operation, cost-effectiveness and reproducible results. It can control the speed, and suitable in wet and dry conditions on a wide range of ferrite materials [104].

Xia et al. [105] used a BM method to prepare soft/hard $xNiFe_2O_4@(1-x)SrCo_{0.2}Fe_{11.8}O_{19}$ composite, a mixture of $SrCo_{0.2}Fe_{11.8}O_{19}$, $NiC_2O_4{\cdot}2H_2O$, and $FeC_2O_4{\cdot}2H_2O$ had calcined in air successively. 5 ml of C_2H_5OH were put into a ball milling container (stainless steel). The container to mass ratio of the sample was about 1/15. Initially, samples were milled 20 min at RT (300 circles/min). After all these, samples were dried at 80 °C for 4 h. Finally, the $NiFe_2O_4@SrCo_{0.2}Fe_{11.8}O_{19}$ composite was calcined at different temperatures for 2 h. These composites have lower specific saturation magnetization, which is suitable for memory storage devices. Xia J et al. [106] has been reported that the two-step BM process was used to synthesize the soft/hard $Mn_{0.6}Zn_{0.4}Fe_2O_4@Sr_{0.85}Ba_{0.15}Fe_{12}O_{19}$ composites. Three different temperatures 700 °C, 800 °C and 900 °C were used for calcining the samples. Due to the formation of the core–shell structure, a strong exchange-coupling interaction has been analyzed, which is suitable for high-density magnetic recording devices. There is another study about two-step BM ceramic process, where soft/hard $xLi_{0.3}Co_{0.5}Zn_{0.2}Fe_2O_4$ $@(1-x)SrFe_{12}O_{19}$ were prepared at different mass ratios x = 0.1, 0.2, and 0.3 and improve the magnetic properties and enhance of exchange-coupling interactions due to existence of the core–shell structure and uniform phase distribution [107].

6.3. H/S nanofibers

The fibers with a diameter in the range of nanometer are called nanofibers, and they can be produced from different polymers that have suitable physical properties and potentials applications. In several studies, ferrite nanofibers have been fabricated by an electrospinning technique and evaluated controlling the crystallite size and microstructures. Some polymers have been used in the precursor solution. Many researchers have developed nanofibers with a mixed composition of polymer and transition metal precursor, then calcined oxide nanofibers were studied for their microstructure and magnetization behavior [108–111].

Song et al. fabricated the $SrFe_{12}O_{19}/Ni_{0.5}Zn_{0.5}Fe_2O_4$ nanofiber ferrite with different mass ratio (1:9, 2:8, 3:7, 4:6, 5:5, 6:4, 7:3, 8:2 and 9:1) electrospinning and calcination process [112]. In this process, a suitable amount of PVP dissolved in ethanol. Then different mass ratios like $Fe(NO_3)_3{\cdot}9H_2O$, $Sr(NO_3)_2$, $C_4H_6NiO_4{\cdot}4H_2O$,

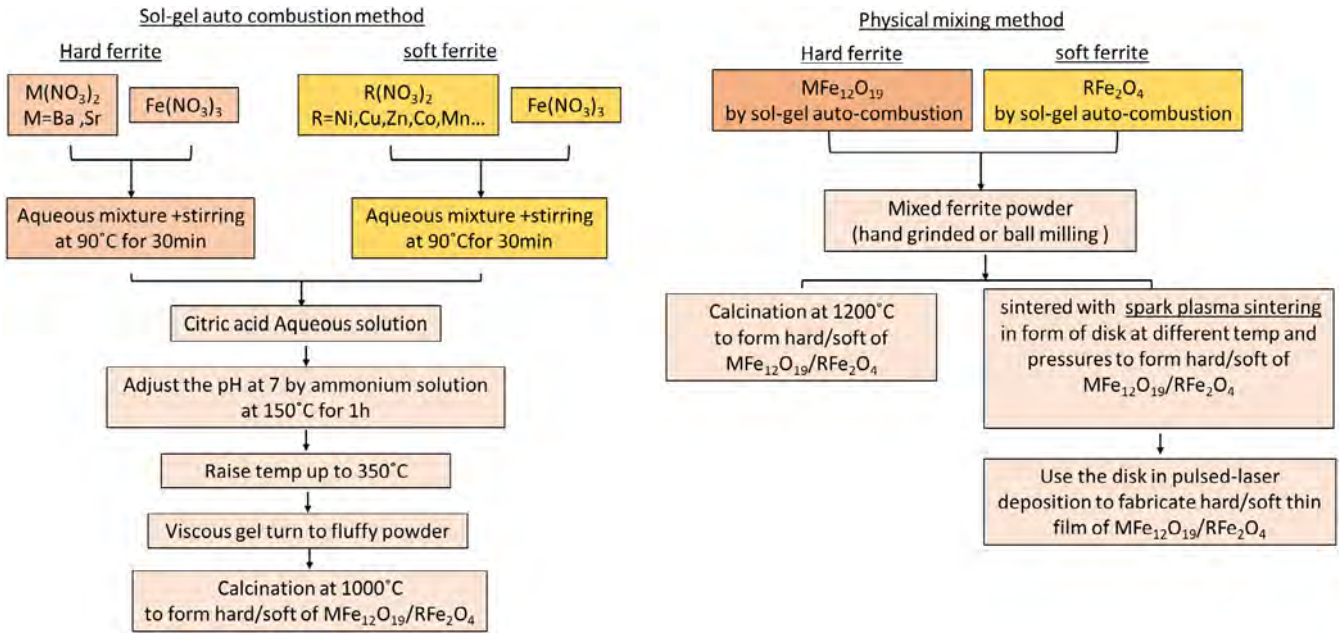

Fig. 2. Synthesis procedure of Hard/soft ferrite Nanocomposites by sol–gel auto-combustion, physical mixing, spark plasma sintering and pulsed-laser deposition methods.

$C_4H_6O_4Zn{\cdot}2H_2O$, and distilled water have been added to the PVP/ethanol solution then stirred for 24 h at RT. A syringe with stainless-steel needle was used to carry the viscous solution, this needle worked as a positive electrode with supply a high-voltage 15 kV, also solution had applied 0.5 mL/h using the electrospinning process. A small piece of Al foil has been positioned in front of the needle tip to accumulate the nanofibers which were then were calcined at different temperatures for 2 h. The grain size, coercivity, and remanence were improved with an exchange-coupling interaction of the composite ferrite nanofibers. Xiang et al. [113] prepared different mass ratios of $BaFe_{12}O_{19}/Ni_{0.5}Zn_{0.5}Fe_2O_4$ ferrite microfibers by gel precursor transformation technique and gel microfibers which were initially dried were placed an alumina crucible followed by calcination at 1000 °C for 3 h. Dong et al. [114] synthesized a core–shell structure of H/S $SrFe_{12}O_{19}$/FeCo nanofibers by reduction process at 300 °C for 0.5 h in a hydrogen atmosphere. The composite nanofibers ($SrFe_{12}O_{19}/CoFe_2O_4$) were calcined at 900 °C for 1 h in the air. $SrFe_{12}O_{19}$/FeCo composite nanofibers were obtained through a mild reduction process. Pan et al. [115] synthesized $CoFe_2O_4/SrFe_{12}O_{19}$ by the electrospinning and calcination process. A unique route was introduced that precursor sol–gel cobalt powder was utilized as a replacement for the cobalt salt. As a result, the samples had shown high M_s and coercivity, and very impressive exchange-coupling interaction of the H/S magnetic nanocomposite was achieved. Xiang et al. [116] fabricated $CoFe_2O_4/CoFe_2$ composite nanofibers using the combined technique of electrospinning with the hydrogen-thermal reduction process. Due to the high mass fraction of $CoFe_2$ coercivity decreased, but remanence and saturation magnetization increased.

6.4. H/S thin films

A layer of material with thickness below 100 nm is classified as thin film. Ferrite thin films have been grown by different approaches including molecular beam epitaxy, magnetron sputtering, evaporation, electroplating, and pulsed laser deposition (PLD) as exposed in Fig. 2. Many ferrite thin films have been investigated as optical, magnetic, and recording media material. Cobalt and Barium ferrites have been studied due to their outstanding and promising properties as well as their good corrosion resistance, better mechanical stability, high coercivity, and low noise [117–119].

It has been reported that the pulsed laser deposition — PLD (KrF laser, $\lambda = 248$ nm) method was used on $MgAl_2O_4$ (MAO) spinel substrates (Crys-Tec, aS = 0.8083 nm) were grown by Fe_3O_4/CFO spinel bilayers. The soft Fe_3O_4 thickness (< 25 nm) and the thick layer of hard CFO were fixed at 25 nm. A solid-state reaction has been used to prepare the $CoFe_2O_4$ target by sintering Fe and Co powders at 1400 °C. The CFO deposition on the substrate at 640 °C, deposition rate at 0.7 nm/min, oxygen pressure 10^{-3} Torr and laser fluence of 1.4 J/cm^2. Therefore, magnetic soft /hard heterostructures of $Fe_3O_4/CoFe_2O_4$ have been synthesis by introducing different thicknesses of soft ferrite from 5 to 25 nm [131]. Chai et al. [132] reported on CoFe thin films with doped NiZn ferrite by using the magnetron sputtering chamber. In the chamber, a three-inch $Co_{50}Fe_{50}$ target has been used along with several $Ni_{0.5}Zn_{0.5}Fe_2O_4$ ferrite chips on the top of the target, cooling and specific pressure are important factors for the substrate. During sputtering, Ar has been used as the inert environment at a flow rate of 16 SCCM. Cui et al. [133] have used a high-vacuum-chamber to synthesize thin film using several sputtering guns, a typical structure of three multilayer films have been represented this formula Mo (50 nm)/HM (z nm)/NM (x nm)/HM (z nm)/Mo (50 nm)/NM (x nm)/Fe (y nm)/(NM¼Mo, Cu or Cr) were deposited onto Si substrate that heated at 923 K. Therefore, Cr, Mo, and Cu are used as NM spacer layer materials and the composition of HM layer is denoted by $Nd_{16}Fe_{71}B_{13}$ (or $Pr_{16}Fe_{71}B_{13}$). Satalkar et al. [134] synthesized ferrites nanocrystals via sol–gel approach, and S/H thin films were deposit onto the targets by using pulsed laser deposition (PLD) method. Various conditions were used to prepare the S/H thin films and deposited on Si substrate. Firstly, the sol–gel approach was used to prepare the $Mg_{0.1}Ni_{0.3}Zn_{0.6}Fe_2O_4$ and $BaFe_{12}O_{19}$ ferrite powders. During the synthesis, citrate-nitrate has been mixed with citric acid as fuel, and mass ratio had taken as 1:1, de-ionized water used to dissolve all the precursors, and alkaline solution was combined to maintain the pH at 7. Finally, dry gel powder gets by heating the solution in the air at 110 °C for about 1 h. The composite

Table 1
Merits and drawbacks of hard-soft synthesis approaches.

Synthesis approach	Merits	Drawbacks	Reference
Single-pot sol–gel	• Inexpensive instruments, • Simple in fabrication, • Cost effective, • Easy to prepare, • There are no complex methods involved, • The yield of the material obtained is high, • The chemical and physical properties of the final product can be tuned by changing the parameters influencing different steps in the preparation process, • Producing uniform and fine soft/hard ferrite powders	After sol–gel process, it needs calcination	[102] [120] [94]
Solid state reaction	• Good crystallinity, • High intensity of XRD peaks	• Requires high temperature to initiate and maintain the chemical reaction which could possibly result in the mass diffusion between core and shell, and destroy the hard and soft phases due to the low thermal stability of the materials at nano scale, results in powders with large particle size, • Limited chemical homogeneity and low sinterability, • Not economic	[91]
Hydrothermal	• Good quality seeds of a fair size, • Low temperature synthesis, • Possibility of obtaining low Crystallite size product	• The impossibility of observing the crystal as it grows, • Employs expensive autoclaves, • Complex, • Takes long time for self-ignition reaction to occur and needs cationic surfactants to remove the impurity like hematite phase (α-Fe_2O_3), • Generates pollution, • It is only applicable for some of the hard/soft material	[121] [122] [123] [124]
Mechanical alloying	• Good crystallinity	• Impurity and lattice strains	[125]
Co-precipitation	• Low temperature, • Easy application, • Simple and versatile	• High possibility of impurity, • Needs annealing,	[126]
Modified flux	• Economical, • Quite suitable for mass production	• High temperature	[91]
Ball milling	• Easy operation, • Large scale production	• When the size of the soft phase is reduced to the correct size, the size of the hard phase is usually over reduced (much less than single domain size), leading to a low $(BH)_{max}$ • It needs expensive instrument	[124]
Self-assembly process	• Easy to operate and eliminate high temperature post reduction to form a soft metal alloy from their corresponding oxides, which may lead to the mass diffusion between core and shell and degrade the exchange coupling. Furthermore, the shell thickness can be easily controlled in the selfassembly method. • Green, • Effective	• Requires a complicated experimental process.	[127] [128]
Physical mixing	• Easy preparation	• Time consuming, • High possibility of impurity • Homogeneity	[92]

in a ratio of 2:1 of hard and soft ferrites was prepared. The powder composite shaped as a pellet form by pressing 3.6 GPa and annealed at 800 °C for 1 day. The pellet was used as a target form and the S/H ferrite thin film was deposited on Si substrate. The PLD setup KrF excimer laser has been used with a pulse of 248 nm and a pulse duration of 20 ns. The substrate was mounted on a rotating axel, and the deposition time was 120 min.

6.5. Spark plasma sintering

In the conventional sintering process, ferrites merged to high density at temperatures not more than 500 °C with 5 min sintering time, whereas grain size remained in the range < 100 nm. In the spark plasma sintering (SPS) technique, DC current pulses have been used to generate internal heat via graphite die enclosing the powder compact. It also allows fast heating and cooling rates, achieving high-density samples with controlled grain growth by consolidating nanopowders [135].

Magnetic hard-soft ferrite-based nanocomposites $SrFe_{12}O_{19-x}$ $CoFe_2O_4$ were prepared by SPS, where x = 5, 10, and 15 wt% were used. In this process particle size has been controlled by the hydrothermal method, then powders of ($SrFe_{12}O_{19}$) and ($CoFe_2O_4$) have been consolidated with SPS process. The SPS parameters were observed such as applied pressure, time, sintering temperature, and exchange-coupled magnetic phases. In the SPS set-up a high-strength carbon die used where placed the powder mixture that is outer diameter is 40 mm and inner diameter 6.3. This powder mixture pressed between two cylinders and applying a DC current, as a result, energy product increases between the S/H magnetic phases. In this process, non-rare-earth-based magnets have achieved significant property [78].

Yi et al. [136] prepared the composite ceramics of $CoFe_2O_4$/Fe_3O_4 with different weight ratios have prepared by SPS method. The following parameters were used for SPS: sintering temperature at 500 °C, with 10 MPa for 5 min. It has been observed that

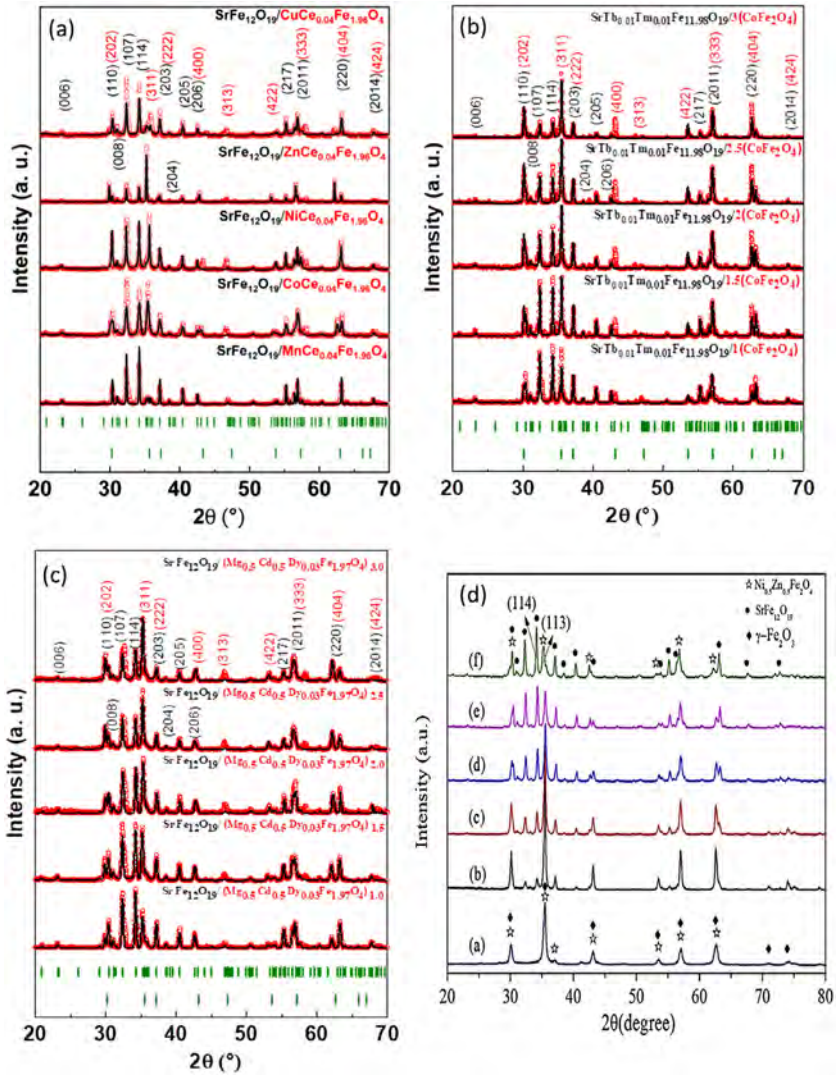

Fig. 3. XRD powder patterns of (*a*) $SrFe_{12}O_{19}/MCe_{0.04}Fe_{1.96}O_4$ (M = Cu, Ni, Mn, Co and Zn), (*b*) $SrTb_{0.01}Tm_{0.01}Fe_{11.98}O_{19}/(CoFe_2O_4)_x$ (x = 1, 1.5, 2, 2.5 and 3), (*c*) $SrFe_{12}O_{19}/Mg_{0.5}Cd_{0.5}Dy_{0.03}Fe_{1.97}O_4$ nanocomposites, (d) $SrFe_{12}O_{19}/Ni_{0.5}Zn_{0.5}Fe_2O_4$ composites [102,101,129,26].

large soft phase content has been achieved and dipolar interaction shows an imperative role throughout the demagnetization process that decreases H_c and M_r. Fei et al. [137] synthesis also $CoFe_2O_4/Fe_3O_4$ nanocomposite by SPS. Initially BM has been used to mix $CoFe_2O_4$ and Fe_3O_4 powders with alcohol for 24 h. Then the mixture was sintered at 200, 300, 400, 500, 600, 700, 800, and 900 °C for 5 min, respectively, under 10 kN pressure using SPS. It was noticed that exchange-coupling at the thin part when the temperature was between 200 to 400 °C and formation of crystalline regions occur when the range was 500 to 700 °C because of the ion diffusion of $CoFe_2O_4/Fe_3O_4$ phases.

6.6. Merits and drawbacks of hard-soft synthesis approaches

The Merits and drawbacks of hard-soft synthesis approaches are stated in Table 1 which showed that none of the mentioned synthesis approach for hard-soft nanocomposite is perfect.

7. Microstructural properties of H/S nanocomposites

7.1. Structural features of H/S ferrite nanocomposites

The H/S magnetic ferrite nanocomposites are materials that crystallize corresponding to hard(H) hexagonal M-type hexaferrite ($P6_3/mmc$ space group) and soft cubic spinel ferrite (S) ($Fd3m$ space group), respectively [64,138]. The general chemical formula of the H/S magnetic ferrite is presented as $AB_{12}O_{19}/MB_2O_4$, (M^{2+} = Ni, Mg, Co, Ca, Zn, and Mn) or a group of these elements with to +2 charge and B is Fe^{+3} ion, whereas A is Sr or Ba (+2) ions [138]. Both A, M and B site in H/S ferrites can be preferentially occupied by (divalent, tetravalent) transition metal and rare earth metals [101]. Accordingly, this will affect electric, magnetic, and microwave properties due to the macrostrain causing the deformation of the hard and soft ferrite structure. The structure of H/S ferrite nanocomposites consists of both cubic and hexagonal phases having the characteristics XRD peaks of M-type hexaferrite as follow (006), (110), (008), (107), (114), (200), (108), (203), (204), (205), (206), (209), (300), (303), (2011), (218), (219), (220), and (2014), and spinel ferrites (inverse and normal spinel) as (220), (311), (222), (400), (422), (511) and (440) as seen in Fig. 3 that is a representative example of H/S ferrite nanocomposites sets [102,120]. However, in most cases, the absence of impurity phases indicates the efficiency of the preparation method for homogeneity of the H/S ferrites formation. Occasionally, a second phase corresponding to α-$Fe_2O_3$was detected [101].

The XRD pattern showed that the intensity of most intense peaks of hexaferrite (hard) (114) and (107) are high due to the presence of larger grains. On the contrary, the intensity of (311)

Table 2
Magnetic and structural parameters for various hard/soft ferrite nanocomposites at 300k.

Hard/soft ferrite nanocomposites	M_s (emu/g)	M_r (emu/g)	H_c (Oe)	$a = b$ (Å)	c (Å)	D_{XRD} (nm)		Ref.
						(Soft	(Hard)	
$(Ba_{0.5}Sr_{0.5}Fe_{12}O_{19})_{0.9}/(NiFe_2O_4)_{0.1}$	64	34	4861	5.82	22.79	44	43	[45]
$(Ba_{0.5}Sr_{0.5}Fe_{12}O_{19})_{0.8}/(NiFe_2O_4)_{0.2}$	61	33	4184	5.81	22.74	42	41	
$(Ba_{0.5}Sr_{0.5}Fe_{12}O_{19})_{0.7}/(NiFe_2O_4)_{0.3}$	52	28	2897	5.85	22.97	36	34	
$(Ba_{0.5}Sr_{0.5}Fe_{12}O_{19})_{0.6}/(NiFe_2O_4)_{0.4}$	51	27	3711	5.82	22.74	33	36	
$SrCo_{0.02}Zr_{0.02}Fe_{11.96}O_{19}/CoFe_2O_4$	64	33	1384	5.88	23.02	22.8	33.3	[102]
$SrCo_{0.02}Zr_{0.02}Fe_{11.96}O_{19}/NiFe_2O_4$	61	32	2617	5.88	23.03	18.7	30.6	
$SrCo_{0.02}Zr_{0.02}Fe_{11.96}O_{19}/ZnFe_2O_4$	66	38	1623	5.88	23.04	28.4	36.5	
$SrCo_{0.02}Zr_{0.02}Fe_{11.96}O_{19}/CuFe_2O_4$	58	30	3212	5.89	23.05	13.1	38.2	
$SrCo_{0.02}Zr_{0.02}Fe_{11.96}O_{19}/MnFe_2O_4$	69	40	2225	5.88	23.03	12.3	35.4	
$SrFe_{12}O_{19}/(Ni_{0.5}Mn_{0.5}Fe_2O_4)_1$	54	26	302	5.87	23.02	14.9	41.4	[96]
$SrFe_{12}O_{19}/(Ni_{0.5}Mn_{0.5}Fe_2O_4)_2$	48	23	252	5.87	23.02	24.1	43.1	
$SrFe_{12}O_{19}/(Ni_{0.5}Mn_{0.5}Fe_2O_4)_3$	46	22	203	5.87	22.99	29.8	42.3	
$SrFe_{11.98}V_{0.02}O_{19}/(Ni_{0.5}Mn_{0.5}Fe_2O_4)_1$	66	23	255	5.87	23.00	28.9	37.1	
$SrFe_{11.98}V_{0.02}O_{19}/(Ni_{0.5}Mn_{0.5}Fe_2O_4)_2$	68	30	261	5.87	22.97	30.9	39.3	
$SrFe_{11.98}V_{0.02}O_{19}/(Ni_{0.5}Mn_{0.5}Fe_2O_4)_3$	69	21	187	5.87	22.99	32.0	40.8	
$SrFe_{11.96}V_{0.04}O_{19}/(Ni_{0.5}Mn_{0.5}Fe_2O_4)_1$	70	24	315	5.87	23.02	15.5	42.0	
$SrFe_{11.96}V_{0.04}O_{19}/(Ni_{0.5}Mn_{0.5}Fe_2O_4)_2$	69	24	278	5.87	22.97	30.2	40.2	
$SrFe_{11.96}V_{0.04}O_{19}/(Ni_{0.5}Mn_{0.5}Fe_2O_4)_3$	70	20	209	5.87	23.00	31.7	42.5	
$Sr_{0.3}Ba_{0.4}Pb_{0.3}Fe_{12}O_{19}/(CuFe_2O_4)_1$	47	21	1507	5.88	23.13	5.6	42.8	[100]
$Sr_{0.3}Ba_{0.4}Pb_{0.3}Fe_{12}O_{19}/(CuFe_2O_4)_2$	43	14	912	5.88	23.12	12.0	32.2	
$Sr_{0.3}Ba_{0.4}Pb_{0.3}Fe_{12}O_{19}/(CuFe_2O_4)_3$	41	12	387	5.87	23.10	31.8	48.6	
$Sr_{0.3}Ba_{0.4}Pb_{0.3}Fe_{12}O_{19}/(CuFe_2O_4)_4$	36	11	339	5.88	23.10	25.4	48.3	
$Sr_{0.3}Ba_{0.4}Pb_{0.3}Fe_{12}O_{19}/(CuFe_2O_4)_5$	32	6	183	5.88	23.12	8.04	38.3	
$(SrFe_{12}O_{19})_{0.8}/(Zn_{0.4}Co_{0.2}Ni_{0.4}Fe_2O_4)_{0.2}$	84	7.2	50	–	–	34	83	[123]
$(SrFe_{12}O_{19})_{0.6}/(Zn_{0.4}Co_{0.2}Ni_{0.4}Fe_2O_4)_{0.4}$	71	3.7	43	-	-	80	78	
$(SrFe_{12}O_{19})_{0.4}/(Zn_{0.4}Co_{0.2}Ni_{0.4}Fe_2O_4)_{0.6}$	91	5.5	54	–	–	58	53	
$(SrFe_{12}O_{19})_{0.2}/(Zn_{0.4}Co_{0.2}Ni_{0.4}Fe_2O_4)_{0.8}$	60	9.6	350	–	–	47	64	
$(BaFe_{11.7}Al_{0.15}Zn_{0.15}O_{19})_{0.3}/(Mn_{0.8}Mg_{0.2}Fe_2O_4)_{0.4}$	50	6	247	5.88	23.03	–	110.16	[130]
$(BaFe_{11.7}Al_{0.15}Zn_{0.15}O_{19})_{0.4}/(Mn_{0.8}Mg_{0.2}Fe_2O_4)_{0.6}$	49	9	390	5.88	23.18	–	74.78	
$(BaFe_{11.7}Al_{0.15}Zn_{0.15}O_{19})_{0.5}/(Mn_{0.8}Mg_{0.2}Fe_2O_4)_{0.5}$	50	12	612	5.88	23.19	–	51.76	
$SrFe_{12}O_{19}(Mg_{0.5}Cd_{0.5}Dy_{0.03}Fe_{1.97}O_4)_{1.0}$	63	28	4738	5.88	23.05	26.1	38.9	[129]
$SrFe_{12}O_{19}(Mg_{0.5}Cd_{0.5}Dy_{0.03}Fe_{1.97}O_4)_{1.5}$	60	24	4186	5.88	23.06	29.6	38.2	
$SrFe_{12}O_{19}(Mg_{0.5}Cd_{0.5}Dy_{0.03}Fe_{1.97}O_4)_{2.0}$	59	22	3604	5.88	23.06	37.8	46.1	
$SrFe_{12}O_{19}(Mg_{0.5}Cd_{0.5}Dy_{0.03}Fe_{1.97}O_4)_{2.5}$	54	20	2171	5.88	23.07	38.2	47.8	
$SrFe_{12}O_{19}(Mg_{0.5}Cd_{0.5}Dy_{0.03}Fe_{1.97}O_4)_{3.0}$	52	17	1400	5.88	23.07	30.8	37.5	

peak of spinel ferrite (soft) was varied according to the mechanism that followed for controlling the content and type of the soft phase [120,130]. The structural parameters have been estimated for hard M-type hexaferrite and soft spinel ferrite individually. Average of crystallite size of (H) and (S) phase for some H/S nanocomposites were listed in Table 2. In some recent reports, lattice constants exhibited a nonlinear variation with the type and fraction of the soft phase [101,139,140]. Whereas, the crystallite sizes of hard phase were almost the twice of the soft phase in order to maximize exchange-spring coupling behavior through an effective coupling of interphase between (H) and (S) phase which stated in several reports such as $[(x)(BaFe_{11.7}Al_{0.15}Zn_{0.15}O_{19})/(1-x)(Mn_{0.8}Mg_{0.2}Fe_2O_4);\ x \leq 0.5]$ [130], $(Ni_{0.65}Zn_{0.35}Fe_2O_4)_x/(BaFe_{12}O_{19})_{1-x}$ $(x = 0.85-0.25)$ [139], $(Ba_{0.5}Sr_{0.5}Fe_{12}O_{19})1-x/(CoFe_2O_4)x$ $(x \leq 0.3)$ [140], $SrCo_{0.02}Zr_{0.02}Fe_{11.96}O_{19}/MFe_2O_4$ (M = Co, Ni, Cu, Mn, and Zn) [102], $SrTb_{0.01}Tm_{0.01}Fe_{11.98}O_{19}/(CoFe_2O_4)_x$ $(x \leq 3.0)$ [101], $SrTb_{0.01}Tm_{0.01}Fe_{11.98}O_{19}/AFe_2O_4$ (A = Ni, Co, Cu, Mn and Zn) [141] and $Sr_{0.3}Ba_{0.4}Pb_{0.3}Fe_{12}O_{19}/(CuFe_2O_4)_x$ with various contents of soft phase $(x \leq 5)$ [100]. On the other hand, some researchers reported that the values of average crystallites size of soft ferrites are near to the crystal size of hard ferrites, representing an improvement in the soft phase crystallite size. The reason for that is the soft ferrite in each composite works to inhibit the hard ferrite growth [94,102].

7.2. Morphological characteristics of H/S ferrite nanocomposites

The morphological and structural characteristics of H/S ferrite nanocomposites were analyzed through Scanning electron microscopy (SEM) and transmission electron microscopy (TEM) as displayed in Figs. 4–6. The morphology of pure hard phase is hexagonal platelet like, while the soft presented roughly spherical shape with sharped edges cubes that cut down from besides and bases. The typical SEM showed the variation in morphology upon growing the quantity and type of soft phase [77,102]. The images presented a clustering of hexagonal platelet particles encapsulated by some small cubic particles, which denotes hexaferrite and spinel ferrite, respectively [102]. It is clear that there is variance in the morphology with altering spinel ferrite type in the degree of conglomerates due to the divergence in spinel behavior in each composition [101,120]. The propensity to agglomeration is observed in the particles as results of magnetic dipole interaction among magnetic hard and soft nanoparticles [77]. The magnetic dipoles of H/S particles are parallel to each other; the mutual attraction between magnetic dipoles results in the re-agglomeration of particles [77]. In addition to the magnetic dipole interaction, the aggregation of particles occurs due to the high magnetic static interaction [77]. Moreover, the particle size distribution is smaller for low content of the soft phase and this leads to better exchange-coupling between grains [94].

TEM micrographs of H/S nanocomposites having aggregated platelet-shaped crystals of different size randomly oriented small spherical grains are shown in Fig. 7. Furthermore, the HR-TEM analysis has been implemented for revealing a typical hexagonal and spinel ferrite symmetry shown by the typical lattice spacing to prove the formation of both (H) and (S) phases [101,120]. SEM and TEM evidence of the surface morphologies and phase formation of $SrCo_{0.02}Zr_{0.02}Fe_{11.96}O_{19}/MFe_2O_4$ (M = Ni, Zn, Mn, Cu, Co, and Zn) and $SrTb_{0.01}Tm_{0.01}Fe_{11.98}O_{19}/(CoFe_2O_4)_x$ $(x \leq 3)$ NCs have been presented by Norah et al. [101,102]. V. Harikrishnan et al.

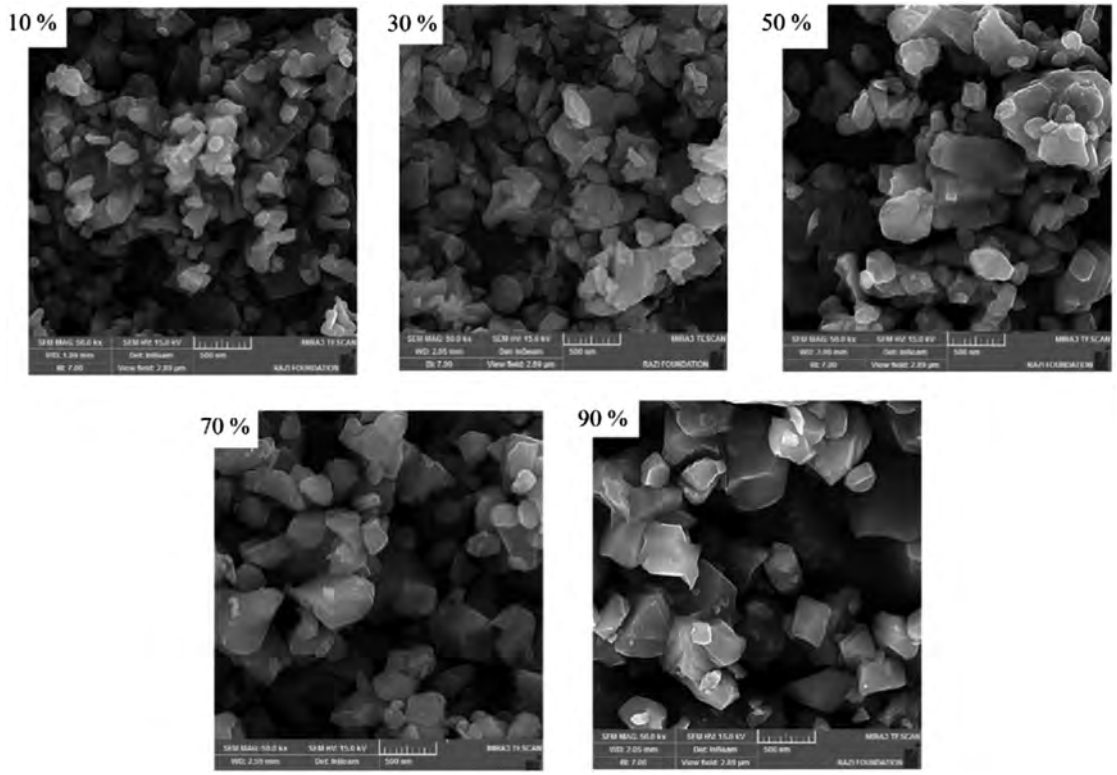

Fig. 4. SEM images of $SrFe_{10}Al_2O_{19}/x(Co_{0.8}Ni_{0.2}Fe_2O_4)$ nanocomposites (x = 10, 30, 50, 70 and 90%) [76].

also analyzed $(Ba_{0.5}Sr_{0.5}Fe_{12}O_{19})_{1-x}(CoFe_2O_4)_x$ ($x \leq 0.3$) using SEM and HR-TEM and found the formation of irregular platelets, revealing the fact that there is the formation of $Ba_{0.5}Sr_{0.5}Fe_{12}O_{19}$ with diacritics circular grains of $CoFe_2O_4$ phase [140]. Likewise, all Hazra et al. Torkian et al. and Pahwa et al. demonstrated the same results for $(Ni_{0.65}Zn_{0.35}Fe_2O_4)_x/(BaFe_{12}O_{19})_{1-x}$ [139], $SrFe_{10}Al_2O_{19}/Co_{0.8}Ni_{0.2}Fe_2O_4$ [94] and $BaFe_{12}O_{19}/NiFe_2O_4$ [142]. Pan et al. and Song et al. exhibited the morphology of H/S nanofibers with different ratios of soft ferrite. They observed the combination of the morphological characteristics from the constituent single ferrites as a continuous linear structure with a uniform diameter. The diameter of these nanofibers was varied when the H/S ratio changed. For higher ratios of soft ferrites, the nanofiber surface became smooth. On the contrary, increasing the hard ferrites ratio, the nanofibers possess a hollow structure with slightly rough surface and the crystallite of the nanofibers grew with the increase of hard ferrite content [115,143].

8. Magnetic properties

H/S ferrites nanocomposites are a new generation of magnetic materials that hold great potential in various applications owing to their many unique properties [129,144]. The integration between the hexaferrite (hard) ($MFe_{12}O_{19}$, M = Sr, Ba, and Pb) and the spinel ferrite (soft) (MFe_2O_4, M = Ni, Co, Zn, or other elements) tuned the magnetic properties by combining a high saturation magnetization (M_s) property related to the soft part with a high magnetic coercivity (H_c) property related to the hard part [145,146]. This combination could generate exchange-coupling behavior. Nevertheless, H/S ferrites nanocomposites include two main interactions, which are the exchange (i.e. interactions between hard and soft grains) and dipolar (i.e. interactions between hard and hard and between soft and soft grains) interactions [146]. These two interactions fundamentally play an important role in deciding the magnetic characteristics in H/S ferrites nanocomposites [89,92]. The magnetization in the remanence state has been greatly administered by the exchange interaction between the adjacent grains of spinel and hexaferrites and their magneto-crystalline anisotropy when the dipolar interactions are insignificant [92]. Because of low magneto-crystalline anisotropy of the spinel ferrite phase, the residual magnetization of hard ferrite will affect on the neighboring grains of the soft ferrite phase in the composite [89]. Hence, the soft magnetization will tend easily to exchange-coupling toward the magnetizations of hard ferrite [89]. In contrast, when the dipole–dipole interactions have a significant impact, the magnetization distribution will be affected by the competition among the exchange interactions and the dipolar coupling, which drive to reduce the magnetic properties [92]. Therefore, if the exchange interaction dominates the dipolar coupling in H/S ferrites nanocomposites, the magnetic properties in composites may be enhanced. Moreover, the particles shape, the average grain sizes of the individual phases, and the distribution of hard and soft ferrite phases in the mixed composition are substantial parameters for emerging the perfect exchange-coupling effect between the spinel and hexaferrite phases [147]. Additionally, when the average size of domain walls in the hard phase is twice or greater than the dimensions of the soft grains can lead to obtain an excellent exchange-coupling effect [144]. Therefore, choosing the appropriate synthesis method has been a critical issue in producing homogeneous powder and desired crystallites size for well-exchange coupled H/S phases [105,144].

To determine the magnetic properties of H/S ferrites nanocomposites such as M_s, M_r, squareness ratio ($SQR = M_r/Ms$), and H_c, VSM is used. A good exchange-coupling between hard and soft magnetic phases can be said to occur when a smooth single M–H hysteresis loop is observed [148,149]. This indicates that the spins of both hard and soft grains at an interfacial layer rotate together in the presence of a magnetic field [145]. However, the appearance of a "bee-waist" or some kind of kink in the M–H

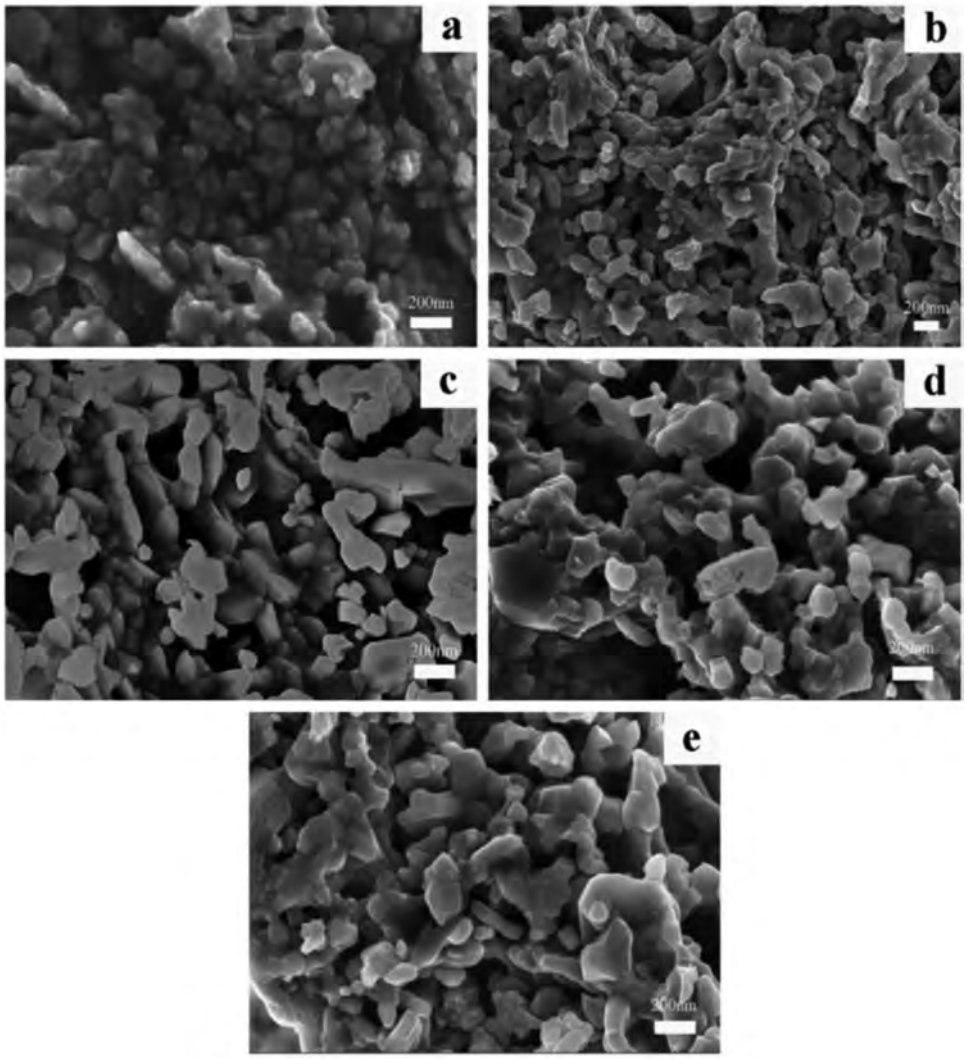

Fig. 5. SEM images of $Ni_{0.5}Zn_{0.5}Fe_2O_4/SrFe_{12}O_{19}$ nanocomposites with different mass ratios. (*a*) 2:1, (*b*) 1:1, (*c*) 1:2, (*d, f*) 1:3, (*e*) 1:4 [77].

hysteresis loop suggests the imperfect exchange-coupling behavior between hard and soft [77,149]. This implies that the spins of hard and soft rotate separately when the magnetic field is applied [149]. To carefully evaluate the exchange-coupling behavior, more analysis should be conducted by making for example the derivation of magnetization data concerning the external magnetic field (*dM/dH*) [77]. Hence, if one single peak was obtained in *dM/dH vs. H* graph, a strong exchange-coupling effect is said has been occurred between the hard and soft ferrite phases [148]. Whereas, if more peaks were detected, a weak exchange-coupling effect has been occurred between the two phases and the dipolar interactions become important [149]. Many investigations have been performed and achieved outstanding results on the exchange-coupling behavior between hard and soft ferrites such as $BaFe_{12}O_{19}/Ni_{0.5}Zn_{0.5}Fe_2O_4$ nanocomposites with 70:30 mass ratio [89,128], $Ni_{0.8}Zn_{0.2}Fe_2O_4/BaFe_{12}O_{19}$ composites at 1:4 ratio [92], $SrFe_{10}Al_2O_{19}/Co_{0.8}Ni_{0.2}Fe_2O_4$ [94], $x(SrFe_{12}O_{19})/(1-x)(NiFe_2O_4)$ nanocomposites ($0.0 \leq x \leq 1.0$) [109], $(Ba_{0.5}Sr_{0.5}Fe_{12}O_{19})1-x/(NiFe_2O_4)x$ [45], and $SrFe_{12}O_{19}/CoFe_2O_4$ at the ratio of 1:4 [150].

According to our previous work, the combination of $SrCo_{0.02}Zr_{0.02}Fe_{11.96}O_{19}$ as hexaferrite type with diverse spinel ferrite types like $CoFe_2O_4$, $CuFe_2O_4$, $NiFe_2O_4$, $MnFe_2O_4$ and $ZnFe_2O_4$ at optimized conditions generated smooth hysteresis loops without any kinks as showing in Fig. 8 [102]. All samples clearly showed one peak in Fig. 9, which refers to the occurrence of a strong exchange-coupling behavior between the two phases [102]. The obtained results suggested to use these materials for different applications such as a microwave field and recording devices [102]. Moreover, H/S ferrite nanocomposites of $SrTb_{0.01}Tm_{0.01}Fe_{11.98}O_{19}/AFe_2O_4$ (where A is Ni, Co, Mn, Cu, and Zn) were synthesized by the sol–gel combustion technique [141]. Generally, an exchange-coupling effect was achieved in these samples and enhanced magnetic properties were noticed in some composites [101]. For instance, the sample which contains Co in soft phase has the highest intensity peak in the graph of *dM/dH* against the magnetic field *H* with the largest values of magnetic parameters, whereas the sample containing the manganese (Mn) in soft part showed the lowest peak in intensity with the smallest values of M_s, M_r, and H_c among all prepared samples [101]. Thus, the excellent exchange-coupling behavior appeared in the $SrTb_{0.01}Tm_{0.01}Fe_{11.98}O_{19}/CoFe_2O_4$ sample [101]. As reported in another study, the duplication of the spinel cobalt ferrite in H/S $SrTb_{0.01}Tm_{0.01}Fe_{11.98}O_{19}/(CoFe_2O_4)_x$ composites ($1.0 \leq x \leq 3.0$) prepared by the sol–gel method [101]. These prepared nanocomposites exhibit well-exchange coupled behavior. The prominent exchange-coupling behavior was detected for the sample that has the highest soft content (i.e. $x = 3$). Furthermore, the saturation magnetization, remanence, and coercivity were increased with the soft content duplication. The reason

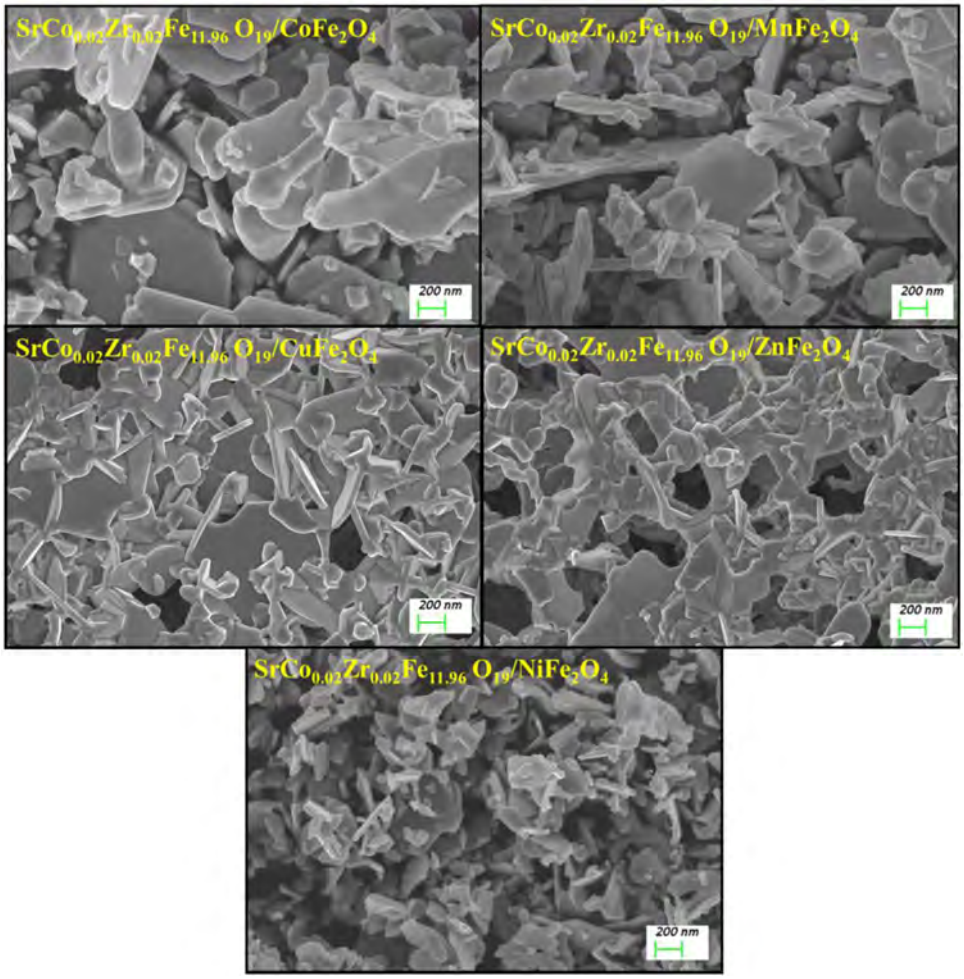

Fig. 6. SEM images of $SrCo_{0.02}Zr_{0.02}Fe_{11.96}O_{19}/MFe_2O_4$ (M = Co, Ni, Cu, Mn and Zn) nanocomposites [102].

for the increase in the values of M_s and M_r is the magnetization nature of spinel cobalt ferrite that is very high [150]. The reason for the increment in H_c value is the dominance of the exchange-coupling effect on their structure compared to the dipolar interaction [101]. However, with an excess increase of spinel content, the soft–soft dipolar interactions progressively influenced on the degree of the exchange-coupling interaction between the two phases, which lead directly to reduce the exchange-coupling interaction and thereby diminish the coercivity [101]. In another research, the exchange-coupling effects in series of $SrFe_{12}O_{19}/MCe_{0.04}Fe_{1.96}O_4$H/S ferrite composites (M = Ni, Cu, Co, Mn, and Zn) were evaluated, and the observed magnetic characteristics were investigated with respect to their structural and morphological features [120]. Among the different fabricated nanocomposites, samples that have Co, and Ni in the soft ferrite phases revealed some shoulders in M–H graphs and double peaks in dM/dH against H plots, indicating the imperfect exchange-coupling behavior in these samples. This proves that the hard/hard and soft/soft interactions (dipolar interactions) existing in these two samples showed a considerable competition with the H/S exchange-coupling interaction, and hence had a big effect in lowering the magnetic properties.

The temperature has a great influence on the values of magnetic parameters [151–156]. Generally, M_s and M_r values increase at lower temperatures in comparison to those at room temperature due to the reduction of thermal fluctuations on magnetic moments and subsequently the enhancement of the super-exchange energy at the diverse sites [155,157]. In contrast, the H_c value falls with reducing the temperature as a result of an inverse correlation between the M_s and coercive field ($H_C \alpha \frac{2K}{\mu_0 \mu_s}$), where the terms μ_0 and K are the magnetic permeability of free space and the magnetocrystalline anisotropy, respectively [155,158]. Additionally, the decrease in the crystallites size could lead to an increment in H_c value and vice versa [159–161]. Magnetic parameters at room and low temperatures for different previously prepared H/S ferrite nanocomposites that display excellent exchange-coupling behavior are represented in Table 2.

The re-distribution of cations in spinel ferrites and the changes in their magnetic traits has occurred when the ferrite is going from the bulk structure form to the nano-sized level [162]. It has been illustrated in a recent study of $SrFe_{12}O_{19}/MnCe_{0.04}Fe_{1.96}O_4$ H/S ferrite nanocomposite that it displayed an uncommon behavior [120,162]. In fact, the bulk Mn spinel ferrites are considered as a normal spinel-type where the divalent cations (Mn^{2+}) and trivalent cations (Fe^{3+}) occupy both the tetrahedral (A) and octahedral (B) sites, respectively [162–165]. Therefore, the $MnFe_2O_4$ in the bulk form exhibits only the B–B exchange interaction and no pertinent effects have occurred from the A–A exchange interaction and the A–B super-exchange interaction [158,162]. With reducing the particles size to the nanoscale level, the three A–A, A–B and B–B interactions will be produced as a result of the structure change from the normal to mixed spinel-type [158,162]. Hence, the inversion of cations will occur in the new structure in which both of Fe^{3+} and Mn^{2+} ions are transferred to both A and B sites, simultaneously [158,165]. Moreover, the cations redistribution degree has been enhanced with the continued reduction

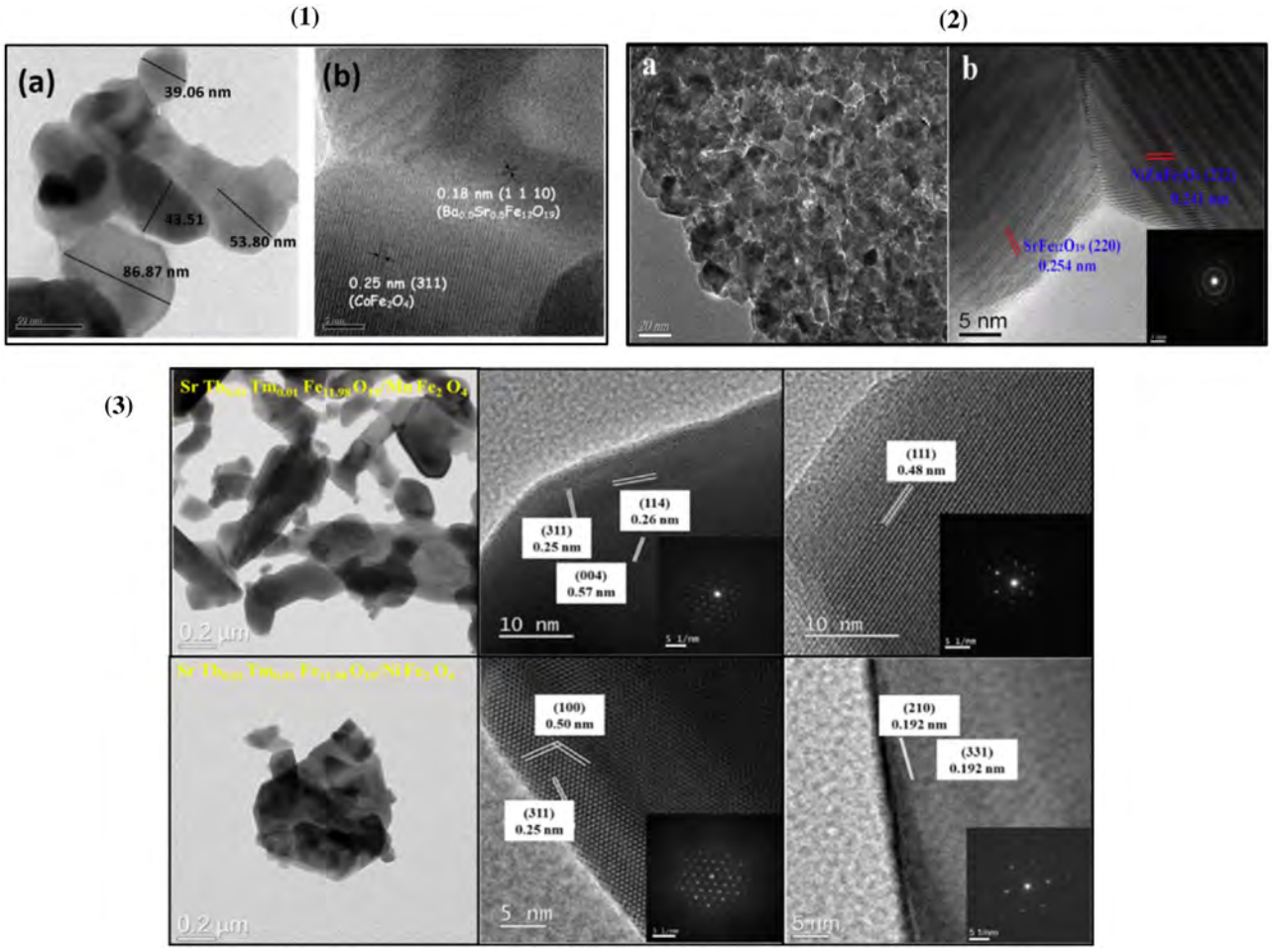

Fig. 7. TEM and HR-TEM of (*1*) $(Ba_{0.5}Sr_{0.5}Fe_{12}O_{19})_{1-x}(CoFe_2O_4)_x$ nanocomposites [140], (*2*) $Ni_{0.5}Zn_{0.5}Fe_2O_4/SrFe_{12}O_{19}$ nanocomposites [77] and (*3*) $SrTb_{0.01}Tm_{0.01}Fe_{11.98}O_{19}/AFe_2O_4$ (where A = Co, Ni, Zn, Cu and Mn) nanocomposites [141].

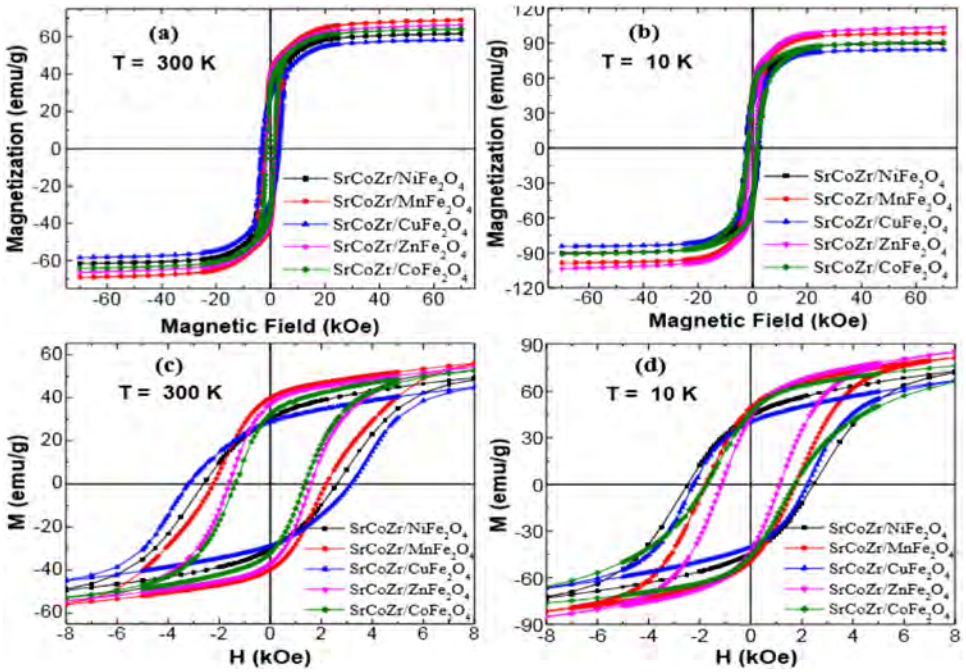

Fig. 8. M–H hysteresis loops for the hard/soft $SrCo_{0.02}Zr_{0.02}Fe_{11.96}O_{19}/MFe_2O_4$ ferrite nanocomposites (where M = Ni, Mn, Cu, Zn, and Co) at (*a, c*) T = 300 K and (*b, d*) T = 10 K [102].

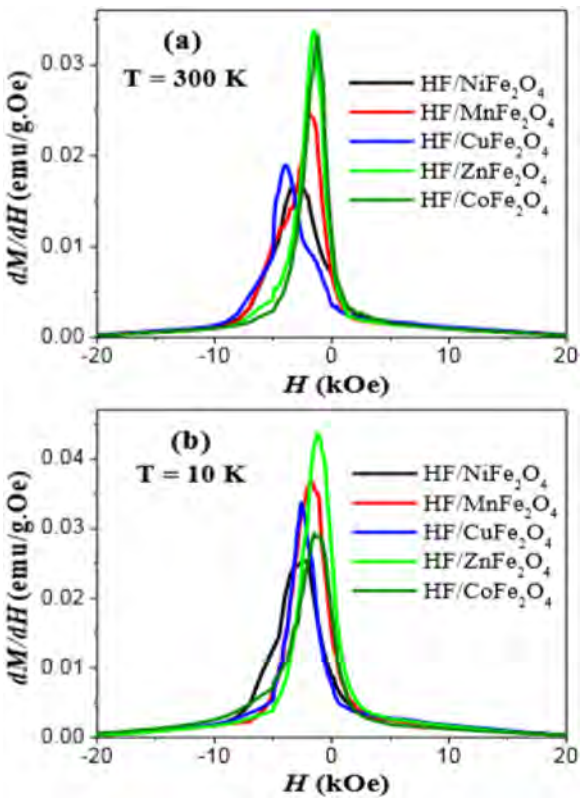

Fig. 9. *dM/dH vs. H* curves for the hard/soft $SrCo_{0.02}Zr_{0.02}Fe_{11.96}O_{19}/MFe_2O_4$ ferrite nanocomposites (where M = Ni, Mn, Cu, Zn, and Co) at (*a*) T = 300 K and (*b*) *T* = 10 K [102].

in particles size that leads to the increment of the effect of A–B exchange interaction, which will be involved in the improvement of magnetic characteristics [142].

The calculation of an effective anisotropy constant (K_{eff}) has been obtained by the expression below [153,166]:

$$K_{eff} = M_s \left(\frac{15b}{4}\right)^{1/2} \quad (1)$$

Where the term *b* is previously deduced from the slope in Eq. (2) [153,166]. The largest value of this constant indicates the largest M_s [161]. Xia et al. [167] have shown that the behavior and the changes in the values of M_s and K_{eff} for the S/H $xNi_{0.5}Zn_{0.5}Fe_2O_4/(1-x)SrFe_{12}O_{19}$ nanocomposites with various x content ($0.1 \leq x \leq 0.3$) are similar in trend. They observed that the highest values of M_s and K_{eff} were obtained for the composite with x = 0.1 ratio, whereas the lowest values of M_s and K_{eff} were estimated for the sample with x = 0.3 [167]. The magnetocrystalline anisotropy field (H_a), which refers to the degree of hard-magnetic traits on the diverse H/S ferrite nanocomposites, is expressed by the following relation [167,168]:

$$H_a = \frac{2K_{eff}}{M_S} \quad (2)$$

The coercive field H_c can be written as below [100,160]:

$$H_c = 0.48\left[\left(\frac{2K_{eff}}{M_S}\right) - NM_S\right] \quad (3)$$

where *N* is known as the demagnetization factor. As mentioned in a previous study [100], the soft content has a great influence on the demagnetization factor. They pointed out that the $Sr_{0.3}Ba_{0.4}Pb_{0.3}Fe_{12}O_{19}/(CuFe_2O_4)_x$ sample that has the largest soft content ratio x = 5 gained the highest value of *N*, whereas the $Sr_{0.3}Ba_{0.4}Pb_{0.3}Fe_{12}O_{19}/(CuFe_2O_4)_x$ sample that has the smallest soft content ratio x = 1 recorded the lowest demagnetization factor [100]. Consequently, the increment of the demagnetization factor leads to diminish the H_c value of samples as a result of the augmentation of soft–soft and hard-hard dipolar interactions [100]. Furthermore, there is a direct proportionality between the M_s and the magnetic moment (n_B) per formula in the Bohr magneton μ_B unit for the prepared samples [164–172]. It can be represented by the following relationship [169–172]:

$$n_B = \frac{M_w \times M_s}{5585} \quad (4)$$

where M_w refers to the molecular weight of nanocomposites and the constant 5585 was called the magnetic factor [169–172]. As discussed by Mansour et al. [97], the type of dominating interaction in the H/S ferrite nanocomposites can be evaluated by the squareness ratio ($SQR = M_r/Ms$). If the *SQR* is larger than 0.5 value, the exchange-coupling is strongly existing between the (H) and (S) phases. Conversely, if the SQR is smaller than 0.5, the dipole–dipole exchange interactions have noticeably dominated, and the exchange-coupling weakly exists in the prepared composite. Additionally, if the *SQR* is equal to 0.5, the two main interactions do not exist (i.e. the magnetic spins order in the (H) and (S) phases in the random state). Thus, the H/S $(x)(Ba\,Fe_{11.7}Al_{0.15}Zn_{0.15}O_{19}) + (1-x)(Mn_{0.8}Mg_{0.2}Fe_2O_4)$ composites (x = 0.3 to 0.5) synthesized by citrate combustion technique showed the values of $M_r/Ms < 0.5$ [172]. This indicates the absence of exchange-coupling interaction in all prepared samples.

Henkel plot (δm vs *H*) method is another way that can be used to detect the degree of dominance of exchange-coupling behavior between (H) and (S) phases and/or dipolar interactions [149,19]. This plot can be obtained by using the expression below [144,173]:

$$\delta m = m_d(H) - [1 - 2m_r(H)] \quad (5)$$

Where, the demagnetization $m_d(H)$ and remanence magnetization $m_r(H)$ are defined by: $m_d(H) = \frac{M_d(H)}{M_d(\infty)}$ and $m_r(H) = \frac{M_r(H)}{M_r(\infty)}$ [45,60]. As reported by Kahnes et al. [174], if the δm is higher than zero (i.e. positive), the exchange-coupling behavior exists. In contrast, if the δm is lower than zero (i.e. negative), the dipolar interaction dominates. The δm vs. *H* plots for the H/S $SrFe_{12}O_{19}/xCoFe_2O_4$ nanocomposites with various x ratio sintered at 700 °C and 900 °C are shown in Fig. 10 [173]. From Fig. 10(a), the positive δm value (exchange-coupling behavior) can be detected only for the nanocomposite with mass ratio (3:1) that is sintered at 700 °C [161,173]. In contrast, the negative peaks (dipolar interaction) were found for the other composites with 1:1 and 1:3 ratios [161,173]. Nevertheless, the nanocomposite with 1:3 ratio still showed the well-exchange-coupling at 900 °C (Fig. 10(b)) [161,173].

The maximum energy product $(BH)_{max}$ is an important result for exchange-coupling H/S ferrite nanocomposites and is considerably used as an indicator for the strength measurement of a permanent magnet [142,175]. For getting $(BH)_{max}$, the magnetic induction *B* can be calculated by using the following equation [176,177]:

$$B = \mu_0(M + H) \quad (6)$$

Where, μ_0 is the vacuum permeability. Then, the *M-H* hysteresis loop will be converted to a *B-H* hysteresis loop [175,178,179]. Hence, $(BH)_{max}$ will be obtained from the second quadrant of the *B-H* curve, which is the largest rectangle area on it as showing in Fig. 11 [178,179]. As indicated in previous studies, the highest values of exchange-coupling behavior in H/S ferrites of $SrFe_{10}Al_2O_{19}/CO_{0.8}Ni_{0.2}Fe_2O_4$ [146] and $BaFe_{12}O_{19}/CaFe_2O_4/CoFe_2O_4$ [180] nanocomposites with diverse mass ratio have

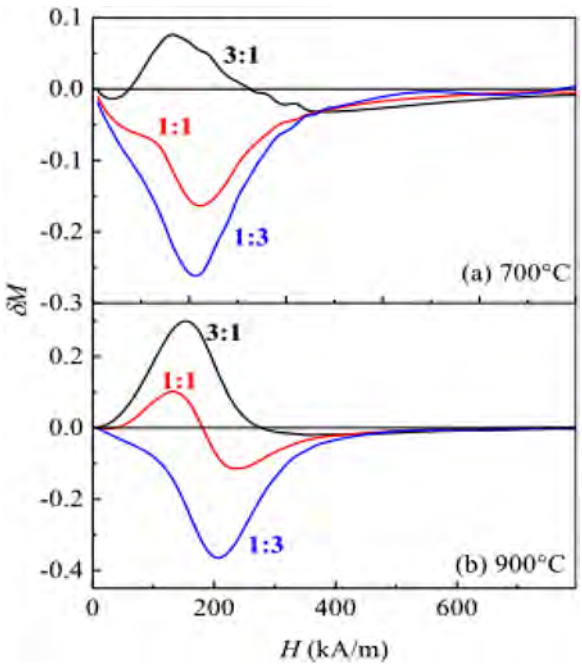

Fig. 10. Henkel plots (δm vs H) for the hard/soft $SrFe_{12}O_{19}/CoFe_2O_4$ nanocomposites for diverse mass ratio that were sintered at (*a*) 700 °C and (*b*) 900 °C [173].

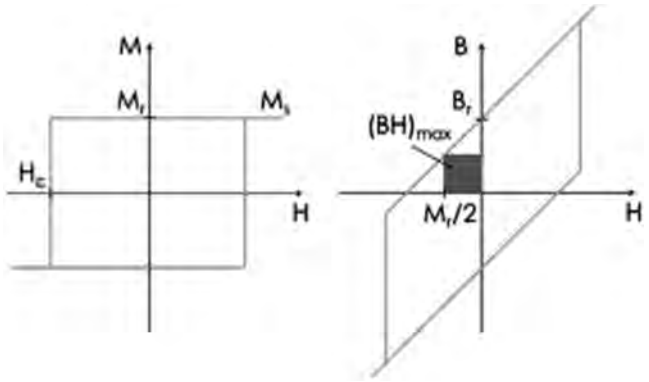

Fig. 11. A schematic for obtaining the maximum energy product $(BH)_{max}$ by converting the M–H hysteresis plot to the B–H hysteresis plot. $(BH)_{max}$ is the largest rectangle area in the second quadrant of the B–H curve [178].

produced maximum values of energy product with values of 29.5 kJ/m^3 for 15 wt% soft content and of 12.1 kJ/m^3 for $0.9BaFe_{12}O_{19}/CaFe_2O_4/0.1CoFe_2O_4$ nanocomposite.

In order to promote the morphological and magnetic characteristics of H/S ferrite composites related to the desired application, many research have been conducted in doping ferrites by transition metals and/or rare earth elements [181,182]. Afshar et al. [103] prepared H/S $SrFe_{12}O_{19-x}/Ni_{0.4}Zn_{0.4}Fe_2O_4$ ferrite composites where x = 0, 10, 20 and 30 wt% via the single-pot sol–gel method. They observed only remarkable one-phase in the hysteresis loop and an enhancement in the magnetic saturation value, which proves the excellent exchange-coupling behavior between the (H) and (S) phases [103]. In another study, it was reported that the increase of spinel ferrite content in H/S ferrite $(Ba_{0.5}Sr_{0.5}Fe_{12}O_{19})_{1-x}(CoFe_2O_4)_x$ composites (where x = 0.1 to 0.3) played a serious part in the degree of the exchange-coupling effect [99]. It is shown that the coercivity and M_s values are high for x = 0.1 and the amount of magnetic coercivity (H_c) is slightly minimized with increasing x content due to the growth inhibition of hard ferrite phase [140]. Song et al. [112] used the electrospinning method with calcination reaction in the fabrication of H/S ferrite nanofibers of $SrFe_{12}O_{19}/Ni_{0.5}Zn_{0.5}Fe_2O_4$. It has been observed that the values of H_c and M_r increase with the decrease in soft content, reaching their maximum values at a certain H/S ratio level. They found that the composite with the H:S ratio of 8:2 exhibits a well exchange-coupling behavior due to the reach of an optimal grains size for the hard and soft ferrite (42 nm and 18 nm for hard and soft phases, respectively), which is well consistent with the theoretical calculations discussed in above parts, especially in the Part 3 – "Exchange-coupling". However, with the further increase in the hard ferrite content to 9:1 mass ratio, the H_c and M_r values start to reduce because of the increment in hard-hard dipolar interactions that obviously compete with the exchange-coupling interactions and thereby reduce the former effect and magnetic properties [112]. In addition, H/S ferrite nanocomposites of $Sr_{0.5}Co_{0.5}Nd_{0.5}Fe_{10.5}O_{19}/NiFe_2O_4$ at diverse mass ratios which are 100:0, 70:30, 50:50, and 30:70 wt.% were synthesized via the self-combustion technique [176]. The co-doping of transition metal (Co^{+2} ions) and rare earth element (Nd^{+3} ions) respectively in the Sr and Fe sites have shown a reduction in the crystallites size of the hard ferrite due to the dissimilarity in ionic radii of different elements and thereby an enhancement in the coercive field has been noticed. It also reported that the achievement of excellent exchange-coupling behavior and the improvement of absorption characteristics particularly in the range of operating frequency (8 to 12 GHz) could be also achieved [176].

9. Microwave and dielectric properties of nanocomposites based on H/S ferrites and mechanisms of the electromagnetic absorption in complex iron oxides

Complex iron oxides or ferrites are perspective candidates for practical applications in high-frequency ranges of electromagnetic radiation. Due to high electrical resistance, temperature, and corrosion stability and coexistence of the insulating and magnetic properties, these materials are widely used as functional media for specific applications. They are used as electromagnetic absorbers [91,177,180]; functional materials for special high-frequency devices such as splitters and circulators [183–185] and antenna technologies [186–189]. Correlation between chemical composition (as such as the chemical composition of the (H) and (S) phases [120,190] and the weight ratio between (H) and (S) phases [89,148]) and microwave properties of the composites based on H/S ferrites attract great attention from fundamental and practical points of view.

9.1. Loss mechanisms in complex iron oxides

Based on Maxwell's relations, two possible types of electromagnetic absorption caused by magnetic and electrical losses can be distinguished. Electrical losses usually arise from the interaction of charges in the material (highly localized and conductive electrons; ions and dipoles) with electromagnetic radiation. In turn, the mechanism of magnetic losses can be related to wave interactions with domain states and spin–orbital magnetic moments [191].

Electrical losses by their features and physical nature can be divided into four main types: *losses due to structural heterogeneity; polarization losses; conductive losses; and ionization losses*. Consequently, three phenomena of the electric field determine or contribute to the occurrence of energy losses in the dielectric: polarization, ionization and electrical conductivity.

Losses on electrical conductivity (conductive losses) are due to the flow of loss current in dielectric materials with a noticeable surface or bulk electrical conductivity. According to the Joule–Lenz law, the flow of current leads to the release of thermal energy and heating of the dielectric, i.e. to irreversible loss of energy of the external field. These losses are negligible in materials with high resistivity, but in dielectrics with low resistivity or in polar materials, operated for example in a humid environment, they should be considered. It is known that the dielectric loss tangent, even at high frequencies, does not fall below 10^{-4}, and electrical conductivity at alternating current is much higher than at direct one. This allows us to assume that in dielectrics, in addition to the conduction mechanism associated with the presence of free charge carriers, other loss mechanisms appear. Obviously, they must be associated with polarization processes. Polarization causes a violation of the thermal motion of particles in the direction of the electric field and leads to energy dissipation or heating of the dielectric. Depending on the type of polarization, relaxation and resonance losses are distinguished.

Relaxation losses are usually associated with the dipole polarization of the dielectric. Dipole polarization is observed in materials containing polar molecules, the bonds between which are small. This is a process associated with the orientation of polar dielectric molecules having a constant dipole moment in the direction of an external electric field and at the same time is associated with the thermal motion of these molecules. This type of loss is observed in polar dielectrics, for example, polymers and ferroelectrics. Polarization losses are observed in the high-frequency region when the hysteresis phenomenon occurs, i.e. the lag of polarization from the change in the external electric field. At the same time, dipole molecules do not "have time" to navigate in a viscous medium of a dielectric following a change in the polarity (direction) of the electric field. At lower frequencies, when the relaxation time is $\tau = 1/\omega$ (ω is the angular frequency of the external electric field), relaxation losses will be small, and with increasing frequency, they will also increase. When the condition $\tau = 1/\omega$ is fulfilled, there will be resonance and losses will increase sharply. With a further increase in the frequency of the external electric field, when $\tau > 1/\omega$, the inertia of the dipole polarization will affect and the dielectric loss tangent $\tan\delta$ will decrease. The relaxation time τ for dipole polarization is 10^{-10}–10^{-6} s. Therefore, relaxation losses are observed in polar dielectrics in 10^{6}–10^{10} Hz. If the dielectric has noticeable conductive losses, then, in accordance with the expression $\tan\delta = 1/R\omega Cs$, they decrease with increasing frequency.

Resonant losses in dielectric materials are caused by ion and electron polarization processes when the frequency of the external electric field coincides with the natural frequency of the ions or electrons. Ion polarization is observed in dielectrics with an ionic type of chemical bond and is caused by separation displacement of oppositely charged ions in an external field. The ion displacement is especially strong in those cases when the ions are relatively weakly coupled to each other and have large electric charges. Thus, the maximum loss in the case of ion polarization is in the frequency range 10^{12}–10^{13} Hz. Electron polarization is the most common type of polarization. It is observed in all dielectrics, regardless of the aggregation state and structure. Electron polarization is due to the displacement in the external field of the electron shells of atoms (ions) from nuclei. The electron polarizability is the higher the larger the size of the atom because an increase in the number of electron layers leads to enhanced shielding of the nucleus by internal electron layers and the bond of the electrons of the outer shell with the nucleus becomes weaker. The electron polarizability of an ion is the smaller the greater its charge because with increasing charge, the radius of the ion decreases and the bond of the electrons with the nucleus is strengthened. Thus, the maximum loss in the case of electron polarization is in the frequency range of 10^{14}–10^{16} Hz.

Ionization losses are characteristic of dielectrics in a gaseous state and also appear in some solid dielectrics containing gas inclusions, such as porous ceramics. Ionization losses are manifested in inhomogeneous electric fields at intensities exceeding the values corresponding to the beginning of ionization of a given gas. In this case, the ionization of gas inclusions occurs, leading to a sharp increase in dielectric loss, heating of the material, and its gradual destruction.

Dielectric losses due to the heterogeneity of the structure are observed in layered plastics, in porous ceramics, in mica derivatives-micanites, mykalex, etc. Due to the diversity of the structure of inhomogeneous dielectrics and the features of their components, there is no general formula for calculating the dielectric loss in this case.

Magnetic losses in ferrites are due to excitation of the magnetic state by the external electromagnetic radiation. Magnetic materials, that absorb EMR, convert field energy into heat, also due to magnetic losses. In the case of an external alternating magnetic field, it will be possible to observe peaks at certain frequencies in the dependency graphs of the imaginary part of the magnetic permeability on frequency. Thus, the mechanisms of resonant EMR absorption are observed. Among the resonance effects in complex iron oxides, two main types can be distinguished: natural ferromagnetic resonance (FMR) [192,193], and resonance of domain boundaries (RDB) [194].

Ferromagnetic resonance (or FMR) arises due to the coincidence of the precession frequency of the total magnetic moment of a ferromagnet particle with the frequency of external microwave radiation. The possibility of such EMR absorption is caused by quantum transitions between discrete Zeeman energy levels that arise due to the presence of a magnetic field. The peculiarity of the resonance in ferromagnets is that due to the strong exchange-coupling between the electron spins, they oscillate in phase under the action of an external alternating field. FMR is interesting because at its frequency the energy loss in the crystal is maximum, which ensures selective absorption of high-frequency energy. The higher the quality of the magnetic crystal, the greater the absorption of energy and the narrower the magnetic resonance band. It was observed that for hard ferrites absorption due to FMR is very sensitive to chemical composition (the level of the substitution of the Fe ions by the diamagnetic ions). Thus in [193] was observed that amplitude–frequency characteristics of the hard ferrites - $BaFe_{12-x}DI_xO_{19}$ solid solutions ($DI = Al^{3+}$ and In^{3+}) have an opposite behavior. For Al-substituted hard ferrites resonance frequency f_{res} increases with an increase in the degree of substitution x: from 51 to 61 GHz in the substitution range from $x = 0.1$ to 1.2, respectively. For In-substituted $BaFe_{12-x}DI_xO_{19}$ f_{res} decreases with an increase in the degree of substitution x: from 50.5 to 27 GHz in the x range from 0.1 to 1.2, respectively. Strong correlation between chemical composition and microwave properties in hard ferrites in the field of NFR is associated with the value of the magneto-crystalline anisotropy as can be seen in Fig. 12 [193].

The working frequency band for hard ferrites is caused by the frequency dispersion range, in which significant changes in magnetic permeability are observed, i.e near the FMR region. Frequency-selective control of EMR characteristics can be achieved using hexagonal ferrites, which are characterized by strong crystalline and magnetic anisotropy, namely by shifting the frequency dispersion region.

The frequency of NFMR for pure $BaFe_{12}O_{19}$ is near 50 GHz and if we neglect the effects of demagnetization, depends on the internal uniaxial anisotropy field H_a

$$\omega_r = \gamma H_a \tag{7}$$

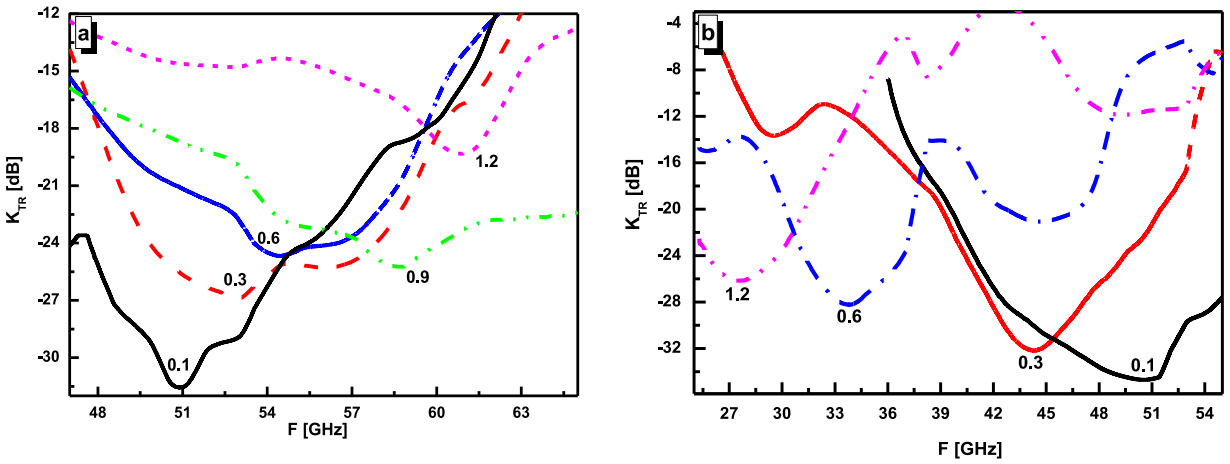

Fig. 12. Frequency dependences of the transmission coefficients in the NFMR area for the $BaFe_{12-x}Al_xO_{19}$ (*a*) and $BaFe_{12-x}In_xO_{19}$ (*b*) with $0.1 \leq x \leq 1.2$ [193].

Where, ω_r is the NFMR frequency, γ is the gyromagnetic ratio. As a rule, the region of NFMR for polycrystalline ferrites is rather wide through the ω_r distribution over crystals (or grains). The effects of demagnetization cannot be ignored when the value of the M_s is sizable. In this case, the demagnetization factors are unequal because of the difference in the crystal shape. If the crystals are magnetized along the hexagonal easy axis by an external magnetic field H_0, the resonant frequency is described by the function:

$$\omega_r = \gamma \left(H_0 + H_a + (N_t - N_l)\, M_s\right) \tag{8}$$

It is assumed that in Eq. (8) the crystallites are in the form of an ellipsoid of rotation, $N_t - N_l$ is the difference between the transverse and longitudinal demagnetizing factors. Hence, we can vary the NFMR parameters (resonant frequency and line width) by controlling the internal parameters H_a and M_s depending on the degree of substitution. FMR phenomenon is usually observed in the region of high frequencies (1000 Hz–100 GHz) where the resonant EMR absorption happens in strong external fields when a ferromagnetic material acquires a single-domain structure. At low values of the field, a multi-domain structure corresponds to lower free energy, thus, it is required to take into consideration the presence of transition regions between the Bloch walls of finite thickness in which the direction of the spontaneous magnetization vector varies continuously. Thereby, the selective EMR absorption in the range of lower frequencies (10–100 Hz) is due to RDB.

Resonance of domain boundaries (RDB). Because any domain wall (e.g. a string or a rigid membrane) is characterized by its own oscillation frequency, with increasing frequency, the forcing EMR approaches the frequency of natural oscillations of a particular domain wall, resulting in resonant absorption of electromagnetic energy. Domain wall dimension has a strong correlation with the average grain size. Moreover, any such domain wall is characterized by its own oscillation frequency due to which there are many peaks of individual walls in the area of the EMR magnetic losses.

Thereby, the higher the degree of dispersion (change in size) and the quantity of crystallite fractions with various grain sizes, the wider the region of the material reflection coefficient, which will be a consequence of the blurring of the RDB peak.

The resonant frequency of the walls is largely determined by their characteristics (the length of the domain wall and its elasticity). Generally, the tendency is that with a decrease in domain size, the length of the domain wall also decreases, while its elasticity increases. The shorter the domain wall and the more elastic it is, the higher the frequency range of resonant absorption of EMR because of the domain wall resonance. Thus, the longer the domain wall and the less elastic it is, the lower the frequency of the resonance of the domain wall. Consequently, a change in the average size of the domain (change in the parameters of the domain wall) makes it possible to vary the resonant frequency of the domain wall. Several factors can affect the size of a domain, the most common of which are: changes in the intensity of exchange interactions caused by magnetic structure frustration (disturbance of the long-range order of exchange interactions), as well as changes in the average crystallite size. These factors can be caused by changes in the chemical composition of the material (substitution of magnetic ions by ions with a larger radius).

9.2. Dielectric and microwave properties of the functional bicomponent nanocomposites based on H/S ferrites

Electrical properties of the complex iron oxides (spinels and hexaferrites) exhibit a large variety from deep insulators to highly conductive materials. Hexagonal ferrites are deep insulators (resistivity hundreds MΩ*cm) if iron oxidation state is Fe^{3+}. For spinels, the same situation can be observed. Dielectric properties are caused by some factors such as high energy of the ionic chemical bond Fe–O; the energy of crystal field; configuration of the Fe^{3+} electronic shells with highly localized d-electrons, etc. There are some factors that dramatically influence on electrical properties (resistivity). One of them is grain boundary transport or conduction of the charge carriers by the defects on the grain surface. In this case the concentration of the defects of the boundary grains and the specific surface area. As a rule for nanostructured ferrites, electrical conductivity higher than for ferrites with the same chemical composition and grains size a few mkm. Divalent Fe^{2+} ions, bound with Fe^{3+} ions, even in a meager amount, significantly reduces the resistance, as a result of which it is extremely easy to observe the exchange (“hopping”) of electrons, which thereby generates current [195]. For this reason, magnetite is an excellent electrical conductor for oxide. Two conduction mechanisms are possible: p-type hole and n-type electron conduction. P-type conductivity is observed in materials with high resistance when one cation is substituted by another, which in turn seeks a lower level of valence, and on the other hand, n-type conductivity is observed when the cation prefers a higher valence. In ferrites, a high concentration of iron (or a lack of oxygen during sintering at high temperatures) causes the formation of Fe^{2+}, which contributes to the occurrence of n-type conductivity, while a lack of iron leads to p-type conductivity, which is negligible in ferrites [196]. Thus, excess of iron should be avoided when the material is to have any electrical applications. It should be noted that high temperatures, required during sintering

to form a dense material, also contribute to an increase in the concentration of Fe^{2+} in the ferrite, however, the addition of manganese or cobalt in a low concentration about 0.02% reduces the resistance by several orders of magnitude [197]. In addition, in polycrystalline ferrites made using the ceramic approach, grains with low resistance are separated by grain walls with high resistance, creating an interfacial polarization which can in turn cause conduction — this will be reduced in larger grained ferrites. It is reported in ferrites containing cobalt, the tendency of Fe^{3+}–Fe^{2+} interaction will be neutralized by the reaction $Fe^{2+} + Co^{3+} - Fe^{3+} + Co^{2+}$, and some other stable multivalent ions such as Mn will have the same effect. The addition of Mn^{3+} is considered to increase the resistivity more than Co^{3+} because it forms a localized stable Mn^{3+}–Fe^{2+} pair, preventing the escape of electrons from Fe^{2+} to other ferric ions [198].

DC-electrical properties strongly correlate with AC-electrical properties. Dielectric properties, along with magnetic properties, are extremely important for most of the high-frequency applications of hexaferrites, especially if they are to become integrated components of a chip. The most significant properties, which become fundamental for many applications, are resistivity and permittivity. As in the case of permeability, a complex dielectric constant can be determined, consisting of real (ε') and imaginary (ε'') parts, from which dielectric resonance and losses can be calculated. Metal cations and oxygen anions make dipoles, producing an intrinsic dielectric polarization. The dominant conduction mechanism in ferrites is the hopping of electrons between ions Fe^{2+} and ions Fe^{3+}.

Pahwa et al. [142] investigated $BaFe_{12}O_{19}$(BaM)/$NiFe_2O_4$ nanocomposites with different weight ratio, which were prepared by two different processing methods (SS — single-step method, when composites were sintered in one step, and PM – (H) and (S) phases were prepared separately and then physically mixed).

As shown in Fig. 13, with an increase in the content of the soft phase ($NiFe_2O_4$), microwave absorption properties decreased at 12–18 GHz in both cases. In addition, it was shown that SS composites exhibit reflection loss (RL) peaks at higher frequencies compared to pure $BaFe_{12}O_{19}$ and PM composites, which means that the SS method is better suited to produce exchange coupled systems.

Microwave properties of exchange-coupled $BaFe_{12}O_{19}/Ni_{0.5}Zn_{0.5}Fe_2O_4$ (NZFO) nanocomposites with different weight ratios were investigated in [57]. RL frequency found to depends on soft phase content (Fig. 14) and maximum loss (−41 dB) was observed for the 70/30 wt% ratio at 13.8 GHz frequency. Obtained results showed that RL values and their frequency strongly depend upon the exchange-coupling.

Mathews et al. [177] showed the results of microwave absorption studies of $(Ba_{0.5}Sr_{0.5}Fe_{12}O_{19})_{1-x}/(NiFe_2O_4)_x$ (x = 0.1−0.4). It was found that minimum RL was higher for sintered composites than for pure (H) and (S) phases (Fig. 15). The most interesting among the studied samples was the $(Ba_{0.5}Sr_{0.5}Fe_{12}O_{19})_{0.6}/(NiFe_2O_4)_{0.4}$ composition since it has demonstrated the best minimum RL values. Han et al. presented studies of the microwave properties of H/S composites $Ni_{0.5}Zn_{0.5}Fe_2O_4/SrFe_{12}O_{19}$ (NZFO/SFO) in relation to the mass ratio (the ratio between the (H) and (S) phases) [77]. Microwave characteristics of NZFO/SFO composites in various mass ratios were established in the range of 2–18 GHz (Fig. 16). It was shown that microwave absorption characteristics are highly dependent on the mass ratio of both NZFO and SFO phases, along with the thickness of sample. It was also found that real permittivity increased with an increase in the proportion of SFO in the compound, which is generally explained by high uniaxial anisotropy and high coercivity of strontium hexaferrite. In addition, real permittivity decreases slightly with increasing frequency from 2 to 18 Hz, which in turn is due to

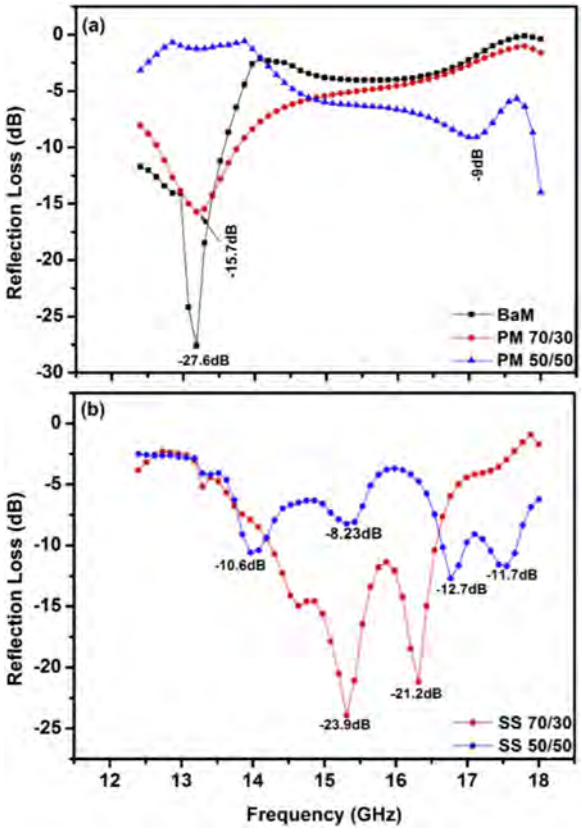

Fig. 13. Reflection loss vs frequency plots for (*a*) BaM, PM 70/30, PM50/50 and (*b*) SS 70/30, SS50/50 nanocomposites [142].

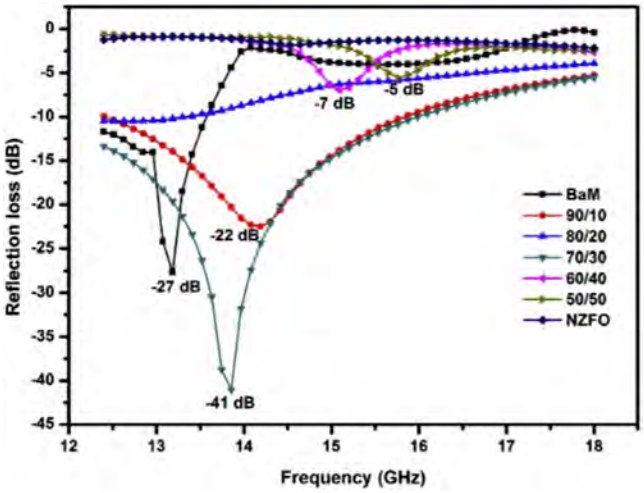

Fig. 14. Reflection loss vs frequency plots for BaM, NZFO and BaM/NZFO nanocomposites for different NZFO content [145].

interface polarization. This means that the mass ratio of soft and hard phases has little effect on the imaginary part of the dielectric constant. The visible multi-resonance peaks on the curve of the imaginary part of the permittivity can be a consequence of spin–spin interaction or interfacial dipole in NZFO/SFO compound. There is also a trend of a strong decrease in the imaginary part of the permeability with increasing frequency. In general, resonance peaks of the permeability of all materials can be divided into two types: resonance peaks associated with natural resonance or caused by the displacement of the domain boundary. The peaks of

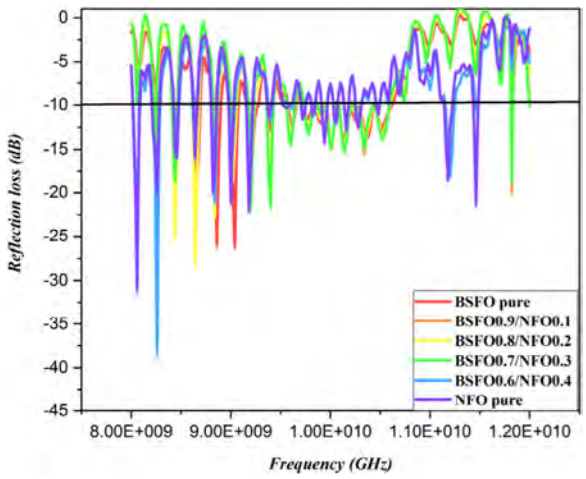

Fig. 15. The reflection loss (RL) values of the pure BSFO, pure NFO and the hard/soft ferrite nanocomposites in different compositions (x = 0.1−0.4) in the X-band region [177].

imaginary permeability in the frequency range of 2–9 GHz can be explained by the displacement of the domain wall resulting from the excitation of the spin-wave and the intrinsic damping effect at the boundary. This can be caused by the formation of excess SFO phase, which reduces the exchange-coupling effect. The mass ratio of the H/S phases determined the exchange-coupling effect and microwave characteristics of the compound. When the mass ratio is 1:3, the effective exchange-coupling effect between SFO and NZFO is obtained, which results in improved microwave absorption characteristics. The RL_{min} value was −47.0 dB, the absorption bandwidth (RL < −10 dB) was 6.4 GHz at 2–18 GHz. Thus, the exchange-coupled NZFO/SFO compounds have great prospects as microwave absorbers.

Correlation between the chemical composition of the soft phase and the microwave properties of the composite was shown in [120]. The authors investigated a series of nanocomposites samples, where $SrFe_{12}O_{19}$ and $MCe_{0.04}Fe_{1.96}O_4$ (M = Cu, Zn, Mn, Co, and Ni) were the hard and the soft phase, respectively. Manganese and nickel spinels displayed the most intensive electromagnetic absorption. The soft phase contains the selected ions with different ionic radii as well as different electronic shell configurations which can be the root of this situation. The ionic to dipole polarization transition in the absorption mechanism was another outcome.

The permittivity value can be influenced critically by the composition of the components in a sample (especially the one belonging to the soft phase). For example, this behavior was observed in the nanocomposites which were composed of $SrM/NiCe_{0.04}Fe_{1.96}O_4$ and $SrM/MnCe_{0.04}Fe_{1.96}O_4$ [120]. The substitution in the A-site in spinel ferrites by the cation M is the main parameter on the permittivity. As stated above, we can explain this by the AC-charge transport features among H/S composites which carry out different microstructural characteristics and/or by the differences among the ionic radii and the electronic shell configuration of the cations which reside in the A-site. When the frequency is below 7 GHz and above 2 GHz, the ionic polarization is the dominant force playing in the permittivity. Upon the presence of an external electric field, the lattice nodes are displaced with a value smaller than that of the lattice constant and hence, there is no change in the frequency range of the dielectric permittivity's real part. However, there is a decrease in the imaginary dielectric permittivity part with rising frequency. We can observe a behavior change from the ionic polarization to a dipole polarization [120].

When the lower frequency exceeds 12 GHz, the dipole polarization dominates the H/S composite $SrM/MCe_{0.04}Fe_{1.96}O_4$ (M = Ni, Cu, Co, Zn and Mn). At low frequencies, the presence of the dipole orientation in the external field is correlated with the dipole polarization and when this force targets to overcome the binding forces among the ions, high loss results in the permittivity are observed. Other materials display similar behavior in the change in the polarization at higher frequencies.

The frequency dependence of the permeability as well as permittivity is correlated with the RL (Fig. 17). The frequency dependence of the RL can be said to display a non-linear trend. On the other hand, the ionic polarization might result in an insufficient RL drop between 7 GHz and 9 GHz. Above 9 GHz, the electromagnetic resonance (EMR) absorption mechanism changes and there is a rise in the RL due to the dipolar polarization. The transition between mechanisms can be observed on the RL curves where the point of inflection appears. In the spinel structure, the electronic shell configuration of the cation of the soft phase residing at the A-site is correlated with the chemical composition which in turn influences the point where the RL inflection occurs.

10. Conclusion and future development trend for the hard/soft ferrites

Exchange-coupled H/S bi-magnetic materials attracted significant attention due to their overall properties that can be tailored by the additional opportunities and flexibility brought by the exchange-coupling interaction between soft and hard magnetic phases [144]. The two main applications where exchange-coupled H/S bi-magnetic materials used are microwave absorbers and

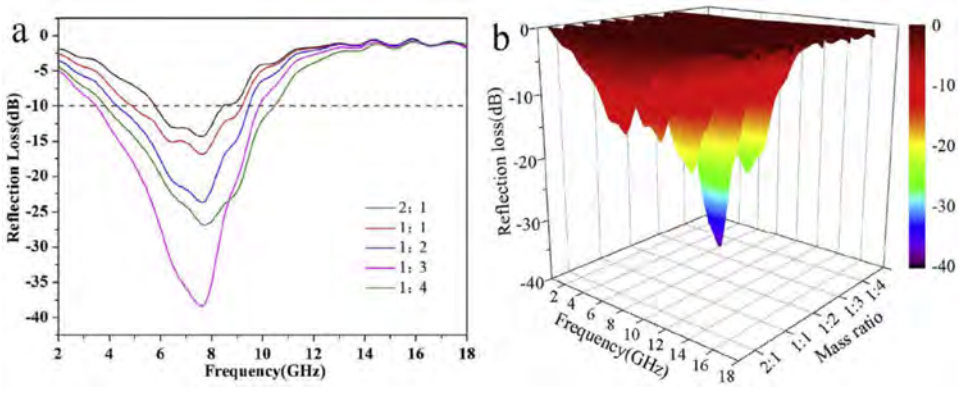

Fig. 16. Reflection loss vs frequency plots for NZFO/SFO composites with different mass ratios [77].

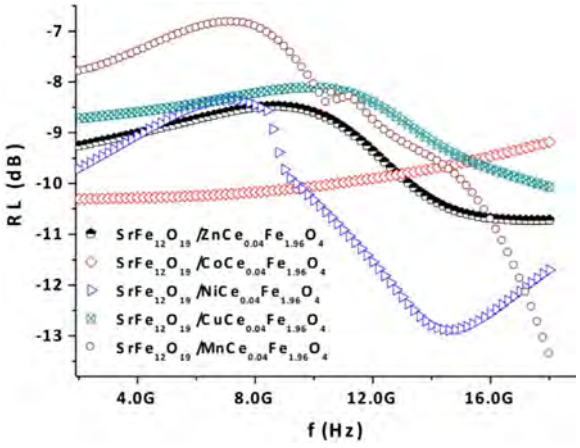

Fig. 17. Frequency dependencies of the reflection losses (RL) of the $SrFe_{12}O_{19}/MCe_{0.04}Fe_{1.96}O_4$ (M = Cu, Ni, Mn, Co and Zn) hard/soft nanocomposites [120].

permanent magnets [75,199]. It is possible to obtain novel or improved properties with the exchange coupling among magnetically soft and hard materials for the following applications and more: data storage, magnetic recording media, energy storage, and biomedical applications including but not limited to drug delivery and diagnostic imaging [200]. The response of the magnetic moment to the microwave application is strengthened by the exchange coupling established between soft and hard magnetic phases, resulting in an enhanced RL above 10 GHz frequency and magnetic permeability exchange resonances [201]. As stated above, the exchange coupling that occurs by the fine mixing of the soft and hard phases also allows us to prepare nanocomposite materials to be used in permanent magnets [201]. In addition to the dipolar and exchange interactions, the grain shape, size and distribution add new and important functionalities in the magnetic characteristics of exchange coupled H/S bi-magnetic ferrite nanocomposites. The establishment of high M_s and high H_c simultaneously has remained as a major challenge for magnetic materials. Therefore, after many attempts, building an exchange-coupled system composed of hard and soft ferrites was found to overcome this hurdle [94]. The high M_s was provided by the soft magnetic phase while the hard phase acted to improve the coercivity. Kneller and Hawig proposed that material with superior magnetic characteristics stated above can be prepared if there is sufficient exchange coupling between both phases, combining the individual high H_c of the hard phase high M_s of the soft phase to yield a highly efficient magnetic energy product [76,94]. Ferrites have been used to obtain permanent magnet materials (PMM) in various applications for decades and there is a constant need to develop novel PMM due to the new technologies. The exchange-coupled H/S ferrite composites are promising materials in this field owing to their high electrical resistivity, great corrosion resistance, enhanced Curie temperature, and economic synthesis [202].

The size, shape, and distribution of grains, as well as the exchange and dipolar interactions introduce significant functions in the magnetic behavior of the two-phase magnetic nanocomposites. A major challenge for the magnetic materials is acquiring high coercivity (Hc) and high saturation of magnetization (Ms) simultaneously. So, many attempts for this confrontation have introduced the design of composite materials consisting of hard and soft magnetic phases [122]. Where the soft magnetic phase provides the high saturation magnetization and the high coercivity is introducing by the hard magnetic phase. Further studies belayed that the high grade of homogeneous mixing of hard and soft ferrite phases was highly important for the fabrication of exchange spring magnet [203–206]. It should be observed that it is not easy to predict conditions for the exchange coupling between hard and soft ferrites since the magnetic properties of the composite are determined not only by the properties of constituent phases but also by the grain sizes and their shapes, as well as by the way in which the hard and soft magnetic phases are interconnected. A close contact required for interphase exchange coupling can be expected in the case of M-type hexaferrites as the hard magnetic phase and the soft magnetic ferrites of spinel structure, which may fit the S blocks of the hexaferrites [143]. The other most important factor is the contribution of both exchange and magnetic anisotropy that determines the remanence and the coercivity. The exchange length of the crystal which is oriented favorably in the presence of the external field sometimes covers some part of the neighboring grains also. The exchange spring behavior has been extensively explored in metallic systems. But still the concept of exchange coupling between soft and hard phases in the field of the oxide nanocomposite permanent magnet is still not realized [206]. The difficulty in the nanocomposite oxide magnet is optimization of magnetic properties due to microstructural complexities [140].

The observation of single-phase reversal behavior in room temperature hysteresis loops as well as remanence enhancement coupled with an increase of the energy product are considered as typical features of exchange-coupled composite systems. However, for hexagonal ferrite-based nanocomposites few studies only demonstrate an increase of remanence. Hence, it is still a matter of controversy, whether or not the magnetic behavior of the SrM/spinel nanocomposites is due to exchange coupling [207].

However, realization of the exchange spring principle in the hard-soft ferrites has encountered difficulties due to the intricate fabrication methods and microstructural complexities [208]. Unfortunately, further complications arise when dealing with polycrystalline nanocomposites [209]. Parameters such as grain shapes, grain (crystallite)-size distribution, or relative orientations of crystallites, which are difficult to quantify and control, play a decisive role [210]. In particular, the structural requirements associated with the effective inter grain coupling, such as interfacial coherency and size of soft grains of the order of a few nanometers, are often hard to meet in large scale production methods as it is difficult to maintain control of the material structure on a nanometric length scale [122].

It is observed the exchange coupled composite shows better magnetic properties as compared to nonexchange coupled ferrites. However, these magnets usually show two-step hysteresis loops indicating that the hard and soft phases have not undergone sufficient exchange coupling at the interfaces. The microwave reflection losses at multiple frequencies are observed in Ku band in exchange coupled composite, while non-exchange coupled system showed losses at single frequency. Such exchange coupled ferrites could be potential candidate for microwave absorber for wide working frequency range [211]. Due to that further investigation is needed to reach this goal. Ferrites are an important class of magnetic materials which exhibit microwave absorption property. Spinel ferrites are used in the megahertz range because of the Snoek's limitation rule, whereas hexaferrites exhibit microwave absorption in the gigahertz range, although the band width is narrow. However, it is difficult for a single material to fulfill all the requirements (such as large absorption peak, wide working frequency range and thin absorption layer) of an ideal radar absorber. Nanocomposites consisting of hard and soft ferrite phase can offer unified systems whose properties are complimentary or even mutually exclusive [212].

Declaration of competing interest

The authors declare that they have no known competing financial interests or personal relationships that could have appeared to influence the work reported in this paper.

Acknowledgments

This work was supported by the Deanship for Scientific Research (Project application No. 2020-164-IRMC) of Imam Abdulrahman Bin Faisal University (IAU — Saudi Arabia).

References

[1] A.-H. Lu, E.L. Salabas, F. Schüth, Magnetic nanoparticles: Synthesis, protection, functionalization, and application, Angew. Chem. Int. Ed. 46 (2007) 1222–1244, http://dx.doi.org/10.1002/anie.200602866.

[2] S.A. Majetich, in: C.C.B.T.-N.M. Koch (Ed.), 10 - Magnetic Nanoparticles and their Applications, second ed., William Andrew Publishing, Norwich, NY, 2007, http://dx.doi.org/10.1016/B978-081551534-0.50012-9.

[3] A.L. Kozlovskiy, M.V. Zdorovets, The study of the structural characteristics and catalytic activity of $Co/CoCo_2O4$ nanowires, Composites Part B: Engineering 191 (2020) 107968, http://dx.doi.org/10.1016/j.compositesb.2020.107968.

[4] O. Gutfleisch, M.A. Willard, E. Brück, C.H. Chen, S.G. Sankar, J.P. Liu, Magnetic materials and devices for the 21st century: Stronger, lighter, and more energy efficient, Adv. Mater. 23 (2011) 821–842, http://dx.doi.org/10.1002/adma.201002180.

[5] A.-H. Lu, W. Schmidt, N. Matoussevitch, H. Bönnemann, B. Spliethoff, B. Tesche, E. Bill, W. Kiefer, F. Schüth, Nanoengineering of a magnetically separable hydrogenation catalyst, Angew. Chem. Int. Ed. 43 (2004) 4303–4306, http://dx.doi.org/10.1002/anie.200454222.

[6] A.L. Kozlovskiy, I.E Kenzhina, M.V. Zdorovets, $FeCo\text{-}Fe_2CoO_4/Co_3O_4$ nanocomposites: Phase transformations as a result of thermal annealing and practical application in catalysis, Ceramics International 46 (8) (2020) 10262–10269, http://dx.doi.org/10.1016/j.ceramint.2020.01.019.

[7] C.A. Ross, Patterned magnetic recording media, Annu. Rev. Mater. Res. 31 (2001) 203–235, http://dx.doi.org/10.1146/annurev.matsci.31.1.203.

[8] M.V. Zdorovets, A.L. Kozlovskiy, Study of phase transformations in $Co/CoCo_2O_4$ nanowires, Journal of Alloys and Compounds 815 (2020) 152450, http://dx.doi.org/10.1016/j.jallcom.2019.152450.

[9] A. Kozlovskiy, Zdorovets, Study of the applicability of directional modification of nanostructures to improve the efficiency of their performance as the anode material of lithium-ion batteries, Materials Research Express 6 (7) (2019) 075066, http://dx.doi.org/10.1088/2053-1591/ab1983.

[10] S. McBain, H. Yiu, J. Dobson, Magnetic nanoparticles for gen and drug delivery, Int. J. Nanomedicine 3 (2008) 169–180, http://dx.doi.org/10.2147/ijn.s1608.

[11] Q.A. Pankhurst, J. Connolly, S.K. Jones, J. Dobson, Applications of magnetic nanoparticles in biomedicine, J. Phys. D: Appl. Phys. 36 (2003) R167–R181, http://dx.doi.org/10.1088/0022-3727/36/13/201.

[12] M.V. Zdorovets, A.L. Kozlovskiy, Investigation of phase transformations and corrosion resistance in $Co/CoCo_2O_4$ nanowires and their potential use as a basis for lithium-ion batteries, Scientific Reports 9 (1) (2019) 16646, http://dx.doi.org/10.1038/s41598-019-53368-y.

[13] S. Hariharan, J. Gass, Superparamagnetism and magneto-caloric effect (MCE) in functional magnetic nanostructures, Adv. Mater. Sci. 10 (2005) 398–402.

[14] X.G. Liu, D.Y. Geng, J.J. Jiang, B. Li, S. Ma, D. Li, W. Liu, Z.D. Zhang, Magnetic properties and large cryogenic low-field magnetocaloric effect of $HoCo_2$ nanoparticles without core/shell structure, J. Nanopart. Res. 12 (2010) 1167–1172, http://dx.doi.org/10.1007/s11051-009-9717-8.

[15] Q. Song, Size and shape-controlled synthesis and superparamagnetic properties of spinel ferrites nanocrystals, 2005, http://hdl.handle.net/1853/7645.

[16] D.S. Mathew, R.-S. Juang, An overview of the structure and magnetism of spinel ferrite nanoparticles and their synthesis in microemulsions, Chem. Eng. J. 129 (2007) 51–65, http://dx.doi.org/10.1016/j.cej.2006.11.001.

[17] C. Bréchignac, P. Houdy, M. Lahmani, Nanomaterials and Nanochemistry, Springer Science & Business Media, 2008, http://dx.doi.org/10.1007/978-3-540-72993-8.

[18] A.J. Cole, V.C. Yang, A.E. David, Cancer theranostics: The rise of targeted magnetic nanoparticles, Trends Biotechnol. 29 (2011) 323–332, http://dx.doi.org/10.1016/j.tibtech.2011.03.001.

[19] D. Vinnik, F. Podgornov, N. Zabeivorota, E. Trofimov, V. Zhivulin, A. Chernukha, M. Gavrilyak, S. Gudkova, D. Zherebtsov, A. Ryabov, Effect of treatment conditions on structure and magnetodielectric properties of barium hexaferrites, J. Magn. Magn. Mater. 498 (2020) 166190, http://dx.doi.org/10.1016/j.jmmm.2019.166190.

[20] V.P. Singh, R. Jasrotia, R. Kumar, P. Raizada, S. Thakur, K.M. Batoo, M. Singh, A current review on the synthesis and magnetic properties of M-type hexaferrites material, World J. Condens. Matter Phys. 8 (2018) 36–61, http://creativecommons.org/licenses/by-nc/4.0/.

[21] V. Mameli, M.S. Angotzi, C. Cara, C. Cannas, Liquid phase synthesis of nanostructured spinel ferrites—A review, J. Nanosci. Nanotechnol. 19 (2019) 4857–4887, http://dx.doi.org/10.1166/jnn.2019.16808.

[22] P. Thakur, D. Chahar, S. Taneja, N. Bhalla, A. Thakur, A review on MnZn ferrites: Synthesis, characterization and applications, Ceram. Int. 46 (2020) 15740–15763, http://dx.doi.org/10.1016/j.ceramint.2020.03.287.

[23] H. Dereje, R.D. Taffa, A.C. Ulpe, C.L. Katharina, L. Bauerfeind, T. .Breedow, W.D. Bahnemann, M. Wark, Photoelectrochemical and theoretical investigations of spinel type ferrites ($M_xFe_{3-x}O_4$) for water splitting: A mini-review, Journal of Photonics for Energy 7 (2016) 012009, http://dx.doi.org/10.1117/1.JPE.7.012009.

[24] M. Yousefi, S. Afghahi, M. Amini, M.B. Torbati, An investigation of structural and magnetic properties of Ce–Nd doped strontium hexaferrite nanoparticles as a microwave absorbent, Mater. Chem. Phys. 235 (2019) 121722, http://dx.doi.org/10.1016/j.matchemphys.2019.121722.

[25] X.F. Meng, Q.X. Hana, Y.J. Sun, Y.F. Liu, Enhancements of saturation magnetization and coercivity in $Ni_{0.5}Zn_{0.5}Fe_2O_4/SrFe_{12}O_{19}$ composite powders by exchange-coupling mechanism, Ceram. Int. 45 (2019) 2504–2508, http://dx.doi.org/10.1007/s10854-019-01527-2.

[26] Q.X. Han, X.F. Meng, C.H. Lu, Exchange-coupled $Ni_{0.5}Zn_{0.5}Fe_2O_4/SrFe_{12}O_{19}$ composites with enhanced microwave absorption performance, J. Alloys Compd. 768 (2018) 742–749, http://dx.doi.org/10.1007/s10854-019-01527-2.

[27] Y.F. Xu, Y.Q. Man, S.T. Xu, F.L. Zan, G.H. Zheng, Z.X. Dai, Obtainment of exchange coupling coefficient of $Ni_{0.6}Zn_{0.4}Fe_2O_4/SrFe_{12}O_{19}$ composites, Mater. Lett. 131 (2014) 203–205, http://dx.doi.org/10.1016/j.matlet.2014.05.187.

[28] S.M.A. Radmanesh, S.A. Seyyed Ebrahimi, Examination the grain size dependence of exchange coupling in oxide-based $SrFe_{12}O_{19}/Ni_{0.7}Zn_{0.3}Fe_2O_4$ nanocomposites, J. Supercond. Nov. Magn. 26 (2013) 2411–2417, http://dx.doi.org/10.1007/s10948-012-1819-3.

[29] A. López-Ortega, M. Estarder, G. Salazar-Alvarez, A.G. Roca, J. Nogués, Applications of exchange coupled bi-magnetic hard/soft and soft/hard magnetic core/shell nanoparticles, Phys. Rep. 553 (2015) 1–32, http://dx.doi.org/10.1016/j.physrep.2014.09.007.

[30] O. Crisan, I. Dan, P. Palade, A.D. Crisan, A. Leca, A. Pantelica, Magnetic phase coexistence and hard–soft exchange coupling in FePt nanocomposite magnets, Nanomaterials 10 (8) (2020) 1618, http://dx.doi.org/10.3390/nano10081618.

[31] G.C.P. Leite, E.F. Chagas, R. Pereira, R.J. Prado, J.T. Terezo, A. Mariella, E. Baggio-Saitovitch, Exchange coupling behavior in bimagnetic $CoFe_2O_4/CoFe_2$ nanocomposite, J. Magn. Magn. 324 (18) (2012) 2711–2716, http://dx.doi.org/10.1016/j.jmmm.2012.03.034.

[32] B.K. Rai, L. Wang, S.R. Mishra, V.V. Nguyen, J.P. Liu, Synthesis and magnetic properties of hard-soft $SrFe_{10}Al_2O_{19}/NiZnFe_2O_4$ ferrite nanocomposites, J. Nanosci. Nanotechnol. 14 (7) (2014) 5272–5277, http://dx.doi.org/10.1166/jnn.2014.8836.

[33] A. Pathania, P. Thakur, A.V. Trukhanov, S.V. Trukhanov, L.V. Panina, U. Lüders, A. Thakur, M. Tomar, V. Gupta, Development of tungsten doped Ni-Zn nano-ferrites with fast response and recovery time for hydrogen gas sensing application, Results Phys. 15 (2019) 102531, http://dx.doi.org/10.1016/j.rinp.2019.102531.

[34] R. Xiong, W. Li, C. Fei, Y. Liu, J. Shi, Exchange-spring behavior in $BaFe_{12}O_{19}\text{-}Ni_{0.5}Zn_{0.5}Fe_2O_4$ nanocomposites synthesized by a combustion method, Ceram. Int. 42 (2016) 11913–11917, http://dx.doi.org/10.1016/j.ceramint.2016.04.114.

[35] J.M. Soares, O.L.A. Conceição, F.L.A. Machado, A. Prakash, S. Radha, A.K. Nigam, Magnetic couplings in $CoFe_2O_4/FeCo–FeO$ core–shell nanoparticles, J. Magn. Magn. 374 (2015) 192–196, http://dx.doi.org/10.1016/j.jmmm.2014.08.015.

[36] W. Feng, H. Liu, P. Hui, H. Yang, J. Li, J.S. Wang, Preparation and properties of $SrFe_{12}O_{19}/ZnFe_2O_4$ core/shell nano-powder microwave absorber, Integr. Ferroelectr. 152 (2014) 120–126, http://dx.doi.org/10.1080/10584587.2014.901882.

[37] D. Li, F. Wang, A. Xia, Afacile way to realize exchange-coupling interaction in hard/soft magnetic composites, J. Magn. Magn. Mater. 41 (2016) 355–358, http://dx.doi.org/10.1016/j.jmmm.2016.05.094.

[38] X.F. Meng, Y.J. Zhu, S. Xu, T. Liu, Facile synthesis of shell–core polyaniline/$SrFe_{12}O_{19}$ composites and magnetic properties, RSC Adv. 6 (2016) 4946–4949, http://dx.doi.org/10.1039/C5RA22200A.

[39] S. Bader, Colloquium: Opportunities in nano magnetism, Rev. Modern Phys. 78 (2006) http://dx.doi.org/10.1103/RevModPhys.78.1.

[40] S. Hazra, N. Ghosh, Preparation of nano ferrites and their applications, J. Nanosci. Nanotechnol. 14 (2014) 1983–2000, http://dx.doi.org/10.1166/jnn.2014.8745.

[41] M.P. Horvath, Microwave applications of soft ferrites, J. Magn. Magn. Mater. 215 (2000) 171–183, http://dx.doi.org/10.1016/S0304-8853(00)00106-2.

[42] V.G. Harris, Modern microwave ferrites, IEEE Trans. Magn. 48 (2012) 31075–31104, http://dx.doi.org/10.1109/TMAG.2011.2180732.

[43] M. Mehdipour, H. Sholrollahi, Comparison of microwave absorption properties of $SrFe_{12}O_{19}$, $SrFe_{12}O_{19}/NiFe_2O_4$ and $NiFe_2O_4$ particles, J. Appl. Phys. 113 (2013) 043906, http://dx.doi.org/10.1063/1.4816089.

[44] A. Hilczer, K. Kowalska, E. Markiewicz, P. Adam, Dielectric and magnetic response of $SrFe_{12}O_{19}$-$CoFe_2O_4$ composites obtained by solid state reaction, Mater. Sci. Eng. B 207 (2016) 47–55, http://dx.doi.org/10.1016/j.mseb.2016.02.003.

[45] S.A. Mathews, D.R. Babu, P. Saravanan, Y. Hayakawa, Microwave absorption studies of $(Ba_{0.5}Sr_{0.5}Fe_{12}O_{19})$1-x/$(NiFe_2O_4)$x hard/soft ferrite nanocomposites, Mater. Chem. Phys. 252 (2020) 123063, http://dx.doi.org/10.1016/j.matchemphys.2020.123063.

[46] Q.X. Han, X.F. Meng, C.H. Lu, Exchange-coupled $Ni_{0.5}Zn_{0.5}Fe_2O_4/SrFe_{12}O_{19}$ composites with enhanced microwave absorption performance, J. Alloys Compd. 768 (2018) 742–749, http://dx.doi.org/10.1016/j.jallcom.2018.07.310.

[47] Q. Ma, Y. Ma, F. Zan, Y. Xu, G. Zheng, Z. Dai, M. Wu, G. Li, Complex exchange anisotropy behavior in Co_3O_4–$Ni_{0.6}Zn_{0.4}Fe_2O_4$ composite with different Co_3O_4 content, Mater. Res. Bull. 51 (2014) 381–388, http://dx.doi.org/10.1016/j.materresbull.2013.12.047.

[48] Y. Slimani, M.A. Almessiere, S. Güner, U. Kurtan, A. Baykal, Impacts of sol-gel auto-combustion and ultrasonication approaches on structural, magnetic, and optical properties of Sm-Tm Co-substituted $Sr_{0.5}Ba_{0.5}Fe_{12}O_{19}$ nanohexaferrites: Comparative study, Nanomaterials 10 (2) (2020) 272, http://dx.doi.org/10.3390/nano10020272.

[49] A. Saini, A. Thakur, P. Thakur, Effective permeability and miniaturization estimation of ferrite-loaded microstrip patch antenna, J. Electron. Mater. 45 (8) (2016) 4162–4170, http://dx.doi.org/10.1007/s11664-016-4634-y.

[50] A. Saini, K. Rana, A. Thakur, P. Thakur, J. Luc, M. Patrick, P. Queffelec, Low loss composite nano ferrite with matching permittivity and permeability in UHF band, Mater. Res. Bull. 76 (2016) 94–99, http://dx.doi.org/10.1016/j.materresbull.2015.12.002.

[51] B.D. Cullity, C.D. Graham, Introduction to Magnetic Materials, second ed., Wiley-IEEE Press, 2008.

[52] A. Manikandan, M. Durka, S.A. Antony, A novel synthesis structural morphological and opto-magnetic characterizations of magnetically separable spinel $Co_xMn_{1-x}Fe_2O_4(0\leq x\leq 1)$ nano-catalysts, J. Supercond. Nov. Magn. 27 (2014) 2841–2857, http://dx.doi.org/10.1007/s10948-014-2771-1.

[53] K.E. Sickafus, J.M. Wills, N.W. Grimes, Structure of spinel, J. Am. Ceram. Soc. 82 (1999) 3279–3292, http://dx.doi.org/10.1111/j.1151-2916.1999.tb02241.x.

[54] M.G. Naseri, B.E. Saion, Crystalization in spinel ferrite nanoparticles, in: E.B.S.E.-Y. Mastai (Ed.), Adv. Cryst. Process, IntechOpen, Rijeka, 2012, pp. 349–380, http://dx.doi.org/10.5772/35731.

[55] M.A. Rafiq, A. Javed, M.N. Rasul, M.A. Khan, A. Hussain, Understanding the structural electronic magnetic and optical properties of spinel MFe2O4 (M = Mn, Co, Ni) ferrites, Ceram. Int. 46 (2020) 4976–4983, http://dx.doi.org/10.1016/j.ceramint.2019.10.237.

[56] J. Gutiérrez-López, E. Rodriguez-Senín, J.Y. Pastor, M.A. Paris, A. Martín, B. Levenfeld, A. Várez, Microstructure, magnetic and mechanical properties of Ni–Zn ferrites prepared by powder injection moulding, Powder Technol. 210 (2011) 29–35, http://dx.doi.org/10.1016/j.powtec.2011.02.008.

[57] C. Jiang, R. Liu, X. Shen, L. Zhu, F. Song, $Ni_{0.5}Zn_{0.5}Fe_2O_4$ nanoparticles and their magnetic properties and adsorption of bovine serum albumin, Powder Technol. 211 (2011) 90–94, http://dx.doi.org/10.1016/j.powtec.2011.03.039.

[58] W. Wenwei, C. Jinchao, W. Xuehang, L. Sen, H. Aigui, $Co_{0.35}Mn_{0.65}Fe_2O_4$ magnetic particles: Preparation and kinetics research of thermal process of the precursor, Powder Technol. 215216 (2012) 200–205, http://dx.doi.org/10.1016/j.powtec.2011.09.048.

[59] R.C. Pullar, Hexagonal ferrite fibres and nanofibres, Solid State Phenom. 241 (2015) 1–68, http://dx.doi.org/10.4028/www.scientific.net/ssp.241.1.

[60] J.J. Went, G.W. Rathenau, E.W. Gorter, G.W. Oosterhout, Ferroxdure, a class of permanent magnetic materials, Philips Tech. Rev. 13 (1952) 194–208.

[61] G.H. Jonker, H.P.J. Wijn, P.B. Braun, Ferroxplana, hexagonal ferromagnetic iron-oxide compounds for very high frequencies, Philips Tech. Rev. 18 (1956).

[62] J. Smit, H.P.J. Wijn, in: L.B.T.-A. in E., E.P. Marton (Eds.), Physical Properties of Ferrites, Academic Press, 1954, pp. 69–136, http://dx.doi.org/10.1016/S0065-2539(08)60132-8.

[63] D. Makovec, M. Komelj, G. Dražić, B. Belec, T. Goršak, S. Gyergyek, D. Lisjak, Incorporation of Sc into the structure of barium-hexaferrite nanoplatelets and its extraordinary finite-size effect on the magnetic properties, Acta Mater. 172 (2019) 84–91, http://dx.doi.org/10.1016/j.actamat.2019.04.050.

[64] R.C. Pullar, Hexagonal ferrites: A review of the synthesis, properties and applications of hexaferrite ceramics, Prog. Mater. Sci. 57 (2012) 1191–1334, http://dx.doi.org/10.1016/j.pmatsci.2012.04.001.

[65] S.V. Trukhanov, A.V. Trukhanov, V.G. Kostishyn, L.V. Panina, A.V. Trukhanov, V.A. Turchenko, D.I. Tishkevich, E.L. Trukhanova, O.S. Yakovenko, L. Matzui, Investigation into the structural features and microwave absorption of doped barium hexaferrites, Dalton Trans. 46 (2017) http://dx.doi.org/10.1039/c7dt01708a.

[66] S.V. Trukhanov, A.V. Trukhanov, V.G. Kostishyn, L.V. Panina, A.V. Trukhanov, V.A. Turchenko, D.I. Tishkevich, E.L. Trukhanova, O.S. Yakovenko, L.Y. Matzui, D.A. Vinnik, D.V. Karpinsky, Effect of gallium doping on electromagnetic properties of barium hexaferrite, J. Phys. Chem. Solids 111 (2017) 142–152, http://dx.doi.org/10.1016/j.jpcs.2017.07.014.

[67] S.S. Veisi, M. Yousefi, M.M. Amini, A.R. Shakeri, M. Bagherzadeh, Magnetic and microwave absorption properties of Cu/Zr doped M-type Ba/Sr hexaferrites prepared via sol–gel auto-combustion method, J. Alloys Compd. 773 (2019) 1187–1194, http://dx.doi.org/10.1016/j.jallcom.2018.09.189.

[68] Z. Li, F. Gao, Chemical bond and hardness of M-, W-type hexagonal barium ferrites, Can. J. Chem. 89 (2011) 573–576, http://dx.doi.org/10.1139/v11-013.

[69] ICDD Card Numbers. 84-1531 ($SrFe_{12}O_{19}$), 84-757 ($BaFe_{12}O_{19}$), and 84-2046 ($PbFe_{12}O_{19}$). International Centre for Diffraction Data (ICDD), Newton Square, PA, USA.

[70] G.A. Jones, S.F.H. Parker, J.G. Booth, D. Simkin, Domain structure of the single crystal hexagonal ferrite, Co/sub2/X, IEEE Trans. Magn. 26 (1990) 2804–2806, http://dx.doi.org/10.1109/20.104880.

[71] A. Tauber, J.S. Megill, J.R. Shappirio, Magnetic properties of $Ba_2Zn_2Fe_{28}O_{46}$ and $Ba_2Co_2Fe_{28}O_{46}$ single crystals, J. Appl. Phys. 41 (1970) 1353–1354, http://dx.doi.org/10.1063/1.1658939.

[72] A.J. Kerecman, A. Tauber, T.R. AuCoin, R.O. Savage, Magnetic properties of $Ba_4Zn_2Fe_{36}O_{60}$ single crystals, J. Appl. Phys. 39 (1968) 726–727, http://dx.doi.org/10.1063/1.2163602.

[73] S. Asiri, S. Güner, A.D. Korkmaz, M. Amir, K.M. Batoo, M.A. Almessiere, H. Gungunes, H. Sözeri, A. Baykal, Magneto-optical properties of $BaCr_yFe_{12-y}O_{19}$ $(0.0\leq y\leq 1.0)$ hexaferrites, J. Magn. Magn. Mater. 451 (2018) 463–472, http://dx.doi.org/10.1016/j.jmmm.2017.11.100.

[74] Ü. Özgür, Y. Alivov, H. Morkoç, Microwave ferrites, part 1: Fundamental properties, J. Mater. Sci., Mater. Electron. 20 (2009) 789–834, http://dx.doi.org/10.1007/s10854-009-9923-2.

[75] A. López-Ortega, M. Estrader, G. Salazar-Alvarez, A.G. Roca, J. Nogués, Applications of exchange coupled bi-magnetic hard/soft and soft/hard magnetic core/shell nanoparticles, Phys. Rep. 553 (2015) 1–32, http://dx.doi.org/10.1016/j.physrep.2014.09.007.

[76] S. Torkian, A. Ghasemi, R.S. Razavi, Magnetic properties of hard-soft $SrFe_{10}Al_2O_{19}/Co_{0.8}Ni_{0.2}Fe_2O_4$ ferrite synthesized by one-pot sol–gel autocombustion, J. Magn. Magn. Mater. 416 (2016) 408–416.

[77] Q. Han, X. Meng, C. Lu, Exchange-coupled $Ni_{0.5}Zn_{0.5}Fe_2O_4/SrFe_{12}O_{19}$ composites with enhanced microwave absorption performance, J. Alloys Compd. 768 (2018) 742–749, http://dx.doi.org/10.1016/j.jallcom.2018.07.310.

[78] P. Jenuš, M. Topole, P. McGuiness, C. Granados-Miralles, M. Stingaciu, M. Christensen, S. Kobe, K. Žužek Rožman, Ferrite-based exchange-coupled hard–soft magnets fabricated by spark plasma sintering, J. Am. Ceram. Soc. 99 (2016) 1927–1934, http://dx.doi.org/10.1111/jace.14193.

[79] P. Jubert, Micromagnetic simulations of exchange-coupled core-shell particulate media, IEEE Trans. Magn. 50 (2014) 1–4, http://dx.doi.org/10.1109/TMAG.2014.2327613.

[80] J.M. Soares, V.B. Galdino, O.L.A. Conceição, M.A. Morales, J.H. de Araújo, F.L.A. Machado, Critical dimension for magnetic exchange-spring coupled core/shell $CoFe_2O_4/CoFe_2$ nanoparticles, J. Magn. Magn. Mater. 326 (2013) 81–84, http://dx.doi.org/10.1016/j.jmmm.2012.08.040.

[81] F.L. Zan, Y.Q. Ma, Q. Ma, G.H. Zheng, Z.X. Dai, M.Z. Wu, G. Li, Z.Q. Sun, X.S. Chen, One-step hydrothermal synthesis and characterization of high magnetization $CoFe_2O_4/Co_{0.7}Fe_{0.3}$ nanocomposite permanent magnets, J. Alloys Compd. 553 (2013) 79–85, http://dx.doi.org/10.1016/j.jallcom.2012.11.120.

[82] F. Liu, J. Zhu, W. Yang, Y. Dong, Y. Hou, C. Zhang, H. Yin, S. Sun, Building nanocomposite magnets by coating a hard magnetic core with a soft magnetic shell, Angew. Chem. Int. Ed. 53 (2014) 2176–2180, http://dx.doi.org/10.1002/anie.201309723.

[83] V. Dupuis, V. Gavrilov-Isaac, S. Neveu, M. Aouadi, S. Abramson, Synthesis and properties of magnetic nanoparticles with tunable magnetic anisotropy energy, MRS Online Proc. Libr. 1708 (2014) 1–6, http://dx.doi.org/10.1557/opl.2014.485.

[84] A. Juhin, A. López-Ortega, M. Sikora, C. Carvallo, M. Estrader, S. Estradé, F. Peiró, M.D. Baró, P. Sainctavit, P. Glatzel, J. Nogués, Direct evidence for an interdiffused intermediate layer in bi-magnetic core–shell nanoparticles, Nanoscale 6 (2014) 11911–11920, http://dx.doi.org/10.1039/C4NR02886D.

[85] S. Li, Z. Han, H. Yang, W. Xu, Y. Cui, L. Yu, S. Feng, Influence of Co/Fe ratios on the structures and the magnetic properties of $Fe_xCo_{1-x}/Co_yFe_{1-y}Fe_2O_4$, J. Magn. Magn. Mater. 309 (2007) 36–39, http://dx.doi.org/10.1016/j.jmmm.2006.06.009.

[86] J. Li, J. Li, L. Chen, Y. Lin, X. Liu, X. Gong, D. Li, Characterization and magnetism of Co-modified γ-Fe_2O_3 core–shell nanoparticles by enhancement using NaOH, J. Magn. Magn. Mater. 374 (2015) 157–163, http://dx.doi.org/10.1016/j.jmmm.2014.08.033.

[87] Q. Song, Z.J. Zhang, Controlled synthesis and magnetic properties of bimagnetic spinel ferrite $CoFe_2O_4$ and $MnFe_2O_4$ nanocrystals with core–shell architecture, J. Am. Chem. Soc. 134 (2012) 10182–10190, http://dx.doi.org/10.1021/ja302856z.

[88] J.-H. Lee, J. Jang, J. Choi, S.H. Moon, S. Noh, J. Kim, J.-G. Kim, I.-S. Kim, K.I. Park, J. Cheon, Exchange-coupled magnetic nanoparticles for efficient heat induction, Nature Nanotechnology 6 (2011) 418–422, http://dx.doi.org/10.1038/nnano.2011.95.

[89] C. Pahwa, S.B. Narang, P. Sharma, Composition dependent magnetic and microwave properties of exchange-coupled hard/soft nanocomposite ferrite, J. Alloys Compd. 815 (2020) 152391, http://dx.doi.org/10.1016/j.jallcom.2019.152391.

[90] X. Liu, W. Zhong, B. Gu, Y. Du, Exchange-coupling interaction in nanocomposite $SrFe_{12}O_{19}/\gamma$-Fe_2O_3 permanent ferrites, J. Appl. Phys. 92 (2002) 1028–1032, http://dx.doi.org/10.1063/1.1487908.

[91] S. Tyagi, H.B. Baskey, R.C. Agarwala, V. Agarwala, T.C. Shami, Development of hard/soft ferrite nanocomposite for enhanced microwave absorption, Ceram. Int. 37 (2011) 2631–2641, http://dx.doi.org/10.1016/j.ceramint.2011.04.012.

[92] D. Roy, C. Shivakumara, P.S. Anil Kumar, Observation of the exchange spring behavior in hard–soft-ferrite nanocomposite, J. Magn. Magn. Mater. 321 (2009) L11–L14, http://dx.doi.org/10.1016/j.jmmm.2008.09.017.

[93] H. Yang, T. Ye, Y. Lin, M. Liu, Exchange coupling behavior and microwave absorbing property of the hard/soft ($BaFe_{12}O_{19}/Y_3Fe_5O_{12}$) ferrites based on polyaniline, Synth. Met. 210 (2015) 245–250, http://dx.doi.org/10.1016/j.synthmet.2015.10.006.

[94] S. Torkian, A. Ghasemi, R.S. Razavi, Magnetic properties of hard-soft $SrFe_{10}Al_2O_{19}/Co_{0.8}Ni_{0.2}Fe_2O_4$ ferrite synthesized by one-pot sol–gel auto-combustion, J. Magn. Magn. Mater. 416 (2016) 408–416, http://dx.doi.org/10.1016/j.jmmm.2016.05.050.

[95] M.A. Almessiere, Y. Slimani, A. Baykal, Structural, morphological and magnetic properties of hard/soft $SrFe_{12-x}V_xO_{19}/(Ni_{0.5}Mn_{0.5}Fe_2O_4)_y$ nanocomposites: Effect of vanadium substitution, J. Alloys Compd. 767 (2018) 966–975, http://dx.doi.org/10.1016/j.jallcom.2018.07.212.

[96] W.H. Meiklejohn, C.P. Bean, New magnetic anisotropy, Phys. Rev. 102 (1956) 1413–1414, http://dx.doi.org/10.1103/PhysRev.102.1413.

[97] R. Rana, P. Pandey, R.P. Singh, D.S. Rana, Positive exchange-bias and giant vertical hysteretic shift in $La_{0.3}Sr_{0.7}FeO_3/SrRuO_3$ bilayers, Sci. Rep. 4 (2014) 4138, http://dx.doi.org/10.1038/srep04138.

[98] J. Nogués, D. Lederman, T.J. Moran, I.K. Schuller, Positive exchange bias in FeF_2-Fe bilayers, Phys. Rev. Lett. 76 (1996) 4624–4627, http://dx.doi.org/10.1103/PhysRevLett.76.4624.

[99] S.K. Mishra, F. Radu, H.A. Dürr, W. Eberhardt, Training-induced positive exchange bias in NiFe/IrMn bilayers, Phys. Rev. Lett. 102 (2009) 177208, http://dx.doi.org/10.1103/PhysRevLett.102.177208.

[100] M.A. Almessiere, Y. Slimani, A. Baykal, Exchange spring magnetic behavior of $Sr_{0.3}Ba_{0.4}Pb_{0.3}Fe_{12}O_{19}/(CuFe_2O_4)_x$ nanocomposites fabricated by a one-pot citrate sol–gel combustion method, J. Alloys Compd. 762 (2018) 389–397, http://dx.doi.org/10.1016/j.jallcom.2018.05.232.

[101] N.A. Algarou, Y. Slimani, M.A. Almessiere, A. Baykal, Exchange-coupling behavior in $SrTb_{0.01}Tm_{0.01}Fe_{11.98}O_{19}/(CoFe_2O_4)_x$ hard/soft nanocomposites, New J. Chem. 44 (2020) 5800–5808, http://dx.doi.org/10.1039/D0NJ00109K.

[102] N.A. Algarou, Y. Slimani, M.A. Almessiere, A. Baykal, S. Guner, A. Manikandan, I. Ercan, Enhancement on the exchange coupling behavior of $SrCo_{0.02}Zr_{0.02}Fe_{11.96}O_{19}/MFe_2O_4$ (M = Co, Ni, Cu, Mn and Zn) as hard/soft magnetic nanocomposites, J. Magn. Magn. Mater. 499 (2020) 166308, http://dx.doi.org/10.1016/j.jmmm.2019.166308.

[103] S.R. Saeedi Afshar, M. Hasheminiasari, S.M. Masoudpanah, Structural, magnetic and microwave absorption properties of $SrFe_{12}O_{19}/Ni_{0.6}Zn_{0.4}Fe_2O_4$ composites prepared by one-pot solution combustion method, J. Magn. Magn. Mater. 466 (2018) 1–6, http://dx.doi.org/10.1016/j.jmmm.2018.06.061.

[104] D. Arcos, R. Valenzuela, M. Vázquez, M. Vallet-Regı, Chemical homogeneity of nanocrystalline Zn–Mn spinel ferrites obtained by high-energy ball milling, J. Solid State Chem. 141 (1998) 10–16, http://dx.doi.org/10.1006/jssc.1998.7882.

[105] J. Xia, Y. Ning, Y. Luo, W. Chen, X. Wu, W. Wu, Q. Li, K. Li, Structural and magnetic properties of soft/hard $NiFe_2O_4$@$SrCo_{0.2}Fe_{11.8}O_{19}$ core/shell composite prepared by the ball-milling-assisted ceramic process, J. Mater. Sci., Mater. Electron. 29 (2018) 13903–13913, http://dx.doi.org/10.1007/s10854-018-9523-0.

[106] J. Xia, Y. Shen, C. Xiao, W. Chen, X. Wu, W. Wu, Q. Wang, J. Li, Structural and magnetic properties of soft/hard $Mn_{0.6}Zn_{0.4}Fe_2O_4$@$Sr_{0.85}Ba_{0.15}Fe_{12}O_{19}$ core/shell composite synthesized by the ball-milling-assisted ceramic process, J. Electron. Mater. 47 (2018) 6811–6820, http://dx.doi.org/10.1007/s11664-018-6584-z.

[107] W. Chen, C. Xiao, C. Huang, X. Wu, W. Wu, Q. Wang, J. Li, K. Zhou, Y. Huang, Exchange-coupling behavior in soft/hard $Li_{0.3}Co_{0.5}Zn_{0.2}Fe_2O_4/SrFe_{12}O_{19}$ core/shell composite synthesized by the two-step ball-milling-assisted ceramic process, J. Mater. Sci., Mater. Electron. 30 (2019) 1579–1590, http://dx.doi.org/10.1007/s10854-018-0429-7.

[108] Z. Zhang, C. Shao, X. Li, C. Wang, M. Zhang, Y. Liu, Electrospun nanofibers of p-type NiO/n-type ZnO heterojunctions with enhanced photocatalytic activity, ACS Appl. Mater. Interfaces 2 (2010) 2915–2923, http://dx.doi.org/10.1021/am100618h.

[109] S.K. Choi, S. Kim, S.K. Lim, H. Park, Photocatalytic comparison of TiO_2 nanoparticles and electrospun TiO_2 nanofibers: Effects of mesoporosity and interparticle charge transfer, J. Phys. Chem. C 114 (2010) 16475–16480, http://dx.doi.org/10.1021/jp104317x.

[110] S. Chuangchote, J. Jitputti, T. Sagawa, S. Yoshikawa, Photocatalytic activity for hydrogen evolution of electrospun TiO_2 nanofibers, ACS Appl. Mater. Interfaces 1 (2009) 1140–1143, http://dx.doi.org/10.1021/am9001474.

[111] Q.P. Pham, U. Sharma, A.G. Mikos, Electrospinning of polymeric nanofibers for tissue engineering applications: A review, Tissue Eng. 12 (2006) 1197–1211, http://dx.doi.org/10.1089/ten.2006.12.1197.

[112] F. Song, X. Shen, M. Liu, J. Xiang, Microstructure, magnetic properties and exchange–coupling interactions for one-dimensional hard/soft ferrite nanofibers, J. Solid State Chem. 185 (2012) 31–36, http://dx.doi.org/10.1016/j.jssc.2011.10.009.

[113] X. Shen, F. Song, J. Xiang, M. Liu, Y. Zhu, Y. Wang, Shape anisotropy, exchange-coupling interaction and microwave absorption of hard/soft nanocomposite ferrite microfibers, J. Am. Ceram. Soc. 95 (2012) 3863–3870, http://dx.doi.org/10.1111/j.1551-2916.2012.05375.x.

[114] J. Dong, Y. Zhang, X. Zhang, Q. Liu, J. Wang, Improved magnetic properties of $SrFe_{12}O_{19}$/FeCo core–shell nanofibers by hard/soft magnetic exchange–coupling effect, Mater. Lett. 120 (2014) 9–12, http://dx.doi.org/10.1016/j.matlet.2014.01.022.

[115] L. Pan, D. Cao, P. Jing, J. Wang, Q. Liu, A novel method to fabricate $CoFe_2O_4/SrFe_{12}O_{19}$ composite ferrite nanofibers with enhanced exchange coupling effect, Nanoscale Res. Lett. 10 (2015) 131, http://dx.doi.org/10.1186/s11671-015-0829-z.

[116] J. Xiang, X. Zhang, J. Li, Y. Chu, X. Shen, Fabrication, characterization, exchange coupling and magnetic behavior of $CoFe_2O_4/CoFe_2$ nanocomposite nanofibers, Chem. Phys. Lett. 576 (2013) 39–43, http://dx.doi.org/10.1016/j.cplett.2013.05.020.

[117] Y. Suzuki, R.B. van Dover, E.M. Gyorgy, J.M. Phillips, V. Korenivski, D.J. Werder, C.H. Chen, R.J. Cava, J.J. Krajewski, W.F. Peck, K.B. Do, Structure and magnetic properties of epitaxial spinel ferrite thin films, Appl. Phys. Lett. 68 (1996) 714–716, http://dx.doi.org/10.1063/1.116601.

[118] T. Tsuchiya, H. Yamashiro, T. Sei, T. Inamura, Preparation of spinel-type ferrite thin films by the dip-coating process and their magnetic properties, J. Mater. Sci. 27 (1992) 3645–3650, http://dx.doi.org/10.1007/BF01151845.

[119] S. Emori, B.A. Gray, H.-M. Jeon, J. Peoples, M. Schmitt, K. Mahalingam, M. Hill, M.E. McConney, M.T. Gray, U.S. Alaan, A.C. Bornstein, P. Shafer, A.T. N'Diaye, E. Arenholz, G. Haugstad, K.-Y. Meng, F. Yang, D. Li, S. Mahat, D.G. Cahill, P. Dhagat, A. Jander, N.X. Sun, Y. Suzuki, B.M. Howe, Coexistence of low damping and strong magnetoelastic coupling in epitaxial spinel ferrite thin films, Adv. Mater. 29 (2017) 1701130, http://dx.doi.org/10.1002/adma.201701130.

[120] N.A. Algarou, Y. Slimani, M.A. Almessiere, F.S. Alahmari, M.G. Vakhitov, D.S. Klygach, S.V. Trukhanov, A.V. Trukhanov, A. Baykal, Magnetic and microwave properties of $SrFe_{12}O_{19}/MCe_{0.04}Fe_{1.96}O_4$ (M = Cu, Ni, Mn, Co and Zn) hard/soft nanocomposites, J. Mater. Res. Technol. 9 (2020) 5858–5870, http://dx.doi.org/10.1016/j.jmrt.2020.03.113.

[121] N. Raghuram, T.S. Rao, N.S. Kumar, et al., BaSrLaFe12O19 nanorods: Optical and magnetic properties, J. Mater. Sci., Mater. Electron. 31 (2020) 8022–8032, http://dx.doi.org/10.1007/s10854-020-03342-6.

[122] A. Manohar, C. Krishnamoorthi, K.C.B. Naidu, et al., Dielectric, magnetic hyperthermia, and photocatalytic properties of ZnFe2O4 nanoparticles synthesized by solvothermal reflux method, Appl. Phys. A 125 (2019) 477, http://dx.doi.org/10.1007/s00339-019-2760-0.

[123] A. Mallikarjuna, S. Ramesh, N. Suresh Kumar, K. Chandra Babu Naidu, K. Venkata Ratnam, H. Manjunatha, B. Parvatheeswara Rao, Structural transformation and high negative dielectric constant behavior in (1−x) (Al0· 2La0· 8TiO3) + (x) (BiFeO3) (x = 0.2–0.8) nanocomposites, Physica E 122 (2020) 114204, http://dx.doi.org/10.1016/j.physe.2020.114204.

[124] N. Raghuram, T. Subba Rao, K. Chandra Babu Naidu, Investigations on functional properties of hydrothermally synthesized Ba1-xSrxFe12O19 (x=0.0-0.8) nanoparticles, Mater. Sci. Semicond. Process. 94 (2019) 136–150, http://dx.doi.org/10.1016/j.mssp.2019.01.037.

[125] U. Naresh, R. Jeevan Kumar, K. Chandra Babu Naidu, Optical, magnetic and ferroelectric properties of Ba0.2Cu0.8-xLaxFe2O4 (x=0.2–0.6) nanoparticles, Ceram. Int. 45 (6) (2019) 7515–7523, http://dx.doi.org/10.1016/j.ceramint.2019.01.044.

[126] L. Zhang, Z. Li, Synthesis and characterization of $SrFe_{12}O_{19}/CoFe_2O_4$ nanocomposites with core–shell structure, J. Alloys Compd. 469 (2009) 422–426, http://dx.doi.org/10.1016/j.jallcom.2008.01.152.

[127] D.M. Andoshe, J.-M. Jeon, S.Y. Kim, H.W. Jang, Two-dimensional transition metal dichalcogenide nanomaterials for solar water splitting, Electron. Mater. Lett. 11 (2015) 323–335, http://dx.doi.org/10.1007/s13391-015-4402-9.

[128] X. Xu, Y.-Ki Hong, J. Park, W. Lee, A.M. Lane, J. Cui, Magnetic self-assembly for the synthesis of magnetically exchange coupled MnBi/Fe–Co composites, J. Solid State Chem. 231 (2015) 108–113, http://dx.doi.org/10.1016/j.jssc.2015.08.019.

[129] N.A. Algarou, Y. Slimani, M.A. Almessiere, S. Rehman, M. Younas, B. Unal, A.D. Korkmaz, M.A. Gondal, A.V. Trukhanov, A. Baykal, I. Nahvi, Developing the magnetic dielectric and anticandidal characteristics of $SrFe_{12}O_{19}/(Mg_{0.5}Cd_{0.5}Dy_{0.03}Fe_{1.97}O_4)_x$ hard/soft ferrite nanocomposites, J. Taiwan Inst. Chem. Eng. 113 (2020) 344–362, http://dx.doi.org/10.1016/j.jtice.2020.07.022.

[130] S.F. Mansour, O.M. Hemeda, M.A. Abdo, W.A. Nada, Improvement on the magnetic and dielectric behavior of hard/soft ferrite nanocomposites, J. Mol. Struct. 1152 (2018) 207–214, http://dx.doi.org/10.1016/j.molstruc.2017.09.089.

[131] G. Lavorato, E. Winkler, B. Rivas-Murias, F. Rivadulla, Thickness dependence of exchange coupling in epitaxial $Fe_3O_4/CoFe_2O_4$ soft/hard magnetic bilayers, Phys. Rev. B 94 (2016) 54405, http://dx.doi.org/10.1103/PhysRevB.94.054405.

[132] G. Chai, N.N. Phuoc, C.K. Ong, Exchange coupling driven omnidirectional rotatable anisotropy in ferrite doped CoFe thin film, Sci. Rep. 2 (2012) 832, http://dx.doi.org/10.1038/srep00832.

[133] W.B. Cui, W. Liu, W.J. Gong, X.H. Liu, S. Guo, F. Yang, Z.H. Wang, Z.D. Zhang, Exchange coupling in hard/soft-magnetic multilayer films with non-magnetic spacer layers, J. Appl. Phys. 111 (2012) 07B503, http://dx.doi.org/10.1063/1.3671774.

[134] M. Satalkar, S.N. Kane, A. Ghosh, S. Raghuvanshi, P. Tapkir, N. Ghodke, D.M. Phase, R.J. Chaudhary, A. Pasko, M. LoBue, F. Mazaleyrat, Study of hard-soft magnetic ferrite films prepared by pulsed laser deposition, J. Phys. Conf. Ser. 534 (2014) 12043, http://dx.doi.org/10.1088/1742-6596/534/1/012043.

[135] R. Breitwieser, U. Acevedo, S. Ammar, R. Valenzuela, Ferrite nanostructures consolidated by spark plasma sintering (SPS), in: Mohindar Singh Seehra (Ed.), Nanostructured Mater. - Fabr. to Appl, 2017, http://dx.doi.org/10.5772/68017.

[136] F. Yi, Magnetic properties of hard ($CoFe_2O_4$)–soft (Fe_3O_4) composite ceramics, Ceram. Int. 40 (2014) 7837–7840, http://dx.doi.org/10.1016/j.ceramint.2013.12.128.

[137] C. Fei, Y. Zhang, Z. Yang, Y. Liu, R. Xiong, J. Shi, X. Ruan, Synthesis and magnetic properties of hard magnetic ($CoFe_2O_4$)–soft magnetic (Fe_3O_4) nano-composite ceramics by SPS technology, J. Magn. Magn. Mater. 323 (2011) 1811–1816, http://dx.doi.org/10.1016/j.jmmm.2011.02.014.

[138] A. Hajalilou, S.A. Mazlan, A review on preparation techniques for synthesis of nanocrystalline soft magnetic ferrites and investigation on the effects of microstructure features on magnetic properties, Appl. Phys. A. 122 (2016) 680, http://dx.doi.org/10.1007/s00339-016-0217-2.

[139] S. Hazra, B.K. Ghosh, M.K. Patra, R.K. Jani, S.R. Vadera, N.N. Ghosh, A novel 'one-pot' synthetic method for preparation of $(Ni_{0.65}Zn_{0.35}Fe_2O_4)_x$ – $(BaFe_{12}O_{19})_{1-x}$ nanocomposites and study of their microwave absorption and magnetic properties, Powder Technol. 279 (2015) 10–17, http://dx.doi.org/10.1016/j.powtec.2015.03.046.

[140] V. Harikrishnan, R. Ezhil Vizhi, A study on the extent of exchange coupling between $(Ba_{0.5}Sr_{0.5}Fe_{12}O_{19})_{1-x}(CoFe_2O_4)_x$ magnetic nanocomposites synthesized by solgel combustion method, J. Magn. Magn. Mater. 418 (2016) 217–223, http://dx.doi.org/10.1016/j.jmmm.2016.03.037.

[141] N.A. Algarou, Y. Slimani, M.A. Almessiere, S. Güner, A. Baykal, I. Ercan, P. Kögerler, Exchange-coupling effect in hard/soft $SrTb_{0.01}Tm_{0.01}Fe_{11.98}O_{19}/AFe_2O_4$ (where A = Co, Ni, Zn, Cu and Mn) composites, Ceram. Int. 46 (2020) 7089–7098, http://dx.doi.org/10.1016/j.ceramint.2019.11.201.

[142] C. Pahwa, S. Mahadevan, S.B. Narang, P. Sharma, Structural, magnetic and microwave properties of exchange coupled and non-exchange coupled $BaFe_{12}O_{19}/NiFe_2O_4$ nanocomposites, J. Alloys Compd. 725 (2017) 1175–1181, http://dx.doi.org/10.1016/j.jallcom.2017.07.220.

[143] F. Song, X. Shen, M. Liu, J. Xiang, One-dimensional $SrFe_{12}O_{19}/Ni_{0.5}Zn_{0.5}Fe_2O_4$ composite ferrite nanofibers and enhancement magnetic property, J. Nanosci. Nanotechnol. 11 (2011) 6979–6985, http://dx.doi.org/10.1166/jnn.2011.4213.

[144] R. Xiong, W. Li, C. Fei, Y. Liu, J. Shi, Exchange-spring behavior in BaFe12O19-$Ni_{0.5}Zn_{0.5}Fe_2O_4$ nanocomposites synthesized by a combustion method, Ceram. Int. 42 (2016) 11913–11917, http://dx.doi.org/10.1016/j.ceramint.2016.04.114.

[145] C. Pahwa, S.B. Narang, P. Sharma, Interfacial exchange coupling driven magnetic and microwave properties of $BaFe_{12}O_{19}/Ni_{0.5}Zn_{0.5}Fe_2O_4$ nanocomposites, J. Magn. Magn. Mater. 484 (2019) 61–66, http://dx.doi.org/10.1016/j.jmmm.2019.03.127.

[146] K. Pubby, P. Sharma, S.B. Narang, Structural, magnetic, dielectric, microwave absorption, and optical characterization of Ni0.1Co0.9(MnZr)xFe2−2xO4/BaySr1−yFe12O19 nanocomposites, J. Mater. Sci., Mater. Electron. 31 (2020) 599–609, http://dx.doi.org/10.1007/s10854-019-02564-7.

[147] T. Schrefl, J. Fidler, H. Kronmüller, Remanence and coercivity in isotropic nanocrystalline permanent magnets, Phys. Rev. B 49 (1994) 6100–6110, http://dx.doi.org/10.1103/PhysRevB.49.6100.

[148] V. Sharma, S. Kumari, B.K. Kuanr, Exchange-coupled hard-soft ferrites; A new microwave material, J. Alloys Compd. 736 (2018) 266–275, http://dx.doi.org/10.1016/j.jallcom.2017.11.113.

[149] Y. Liu, Z. Wang, L. Zhao, J. Zhou, Y. Wang, Improved magnetic and electromagnetic absorption properties of $xSrFe_{12}O_{19}/(1-x)NiFe_2O_4$ composites, J. Am. Ceram. Soc. 102 (2019) 6680–6687, http://dx.doi.org/10.1111/jace.16506.

[150] A. Hilczer, K. Kowalska, E. Markiewicz, A. Pietraszko, B. Andrzejewski, Dielectric and magnetic response of $SrFe_{12}O_{19}$–$CoFe_2O_4$ composites obtained by solid state reaction, Mater. Sci. Eng. B. 207 (2016) 47–55, http://dx.doi.org/10.1016/j.mseb.2016.02.003.

[151] H.C. Fang, Z. Yang, C.K. Ong, Y. Li, C.S. Wang, Preparation and magnetic properties of (Zn–sn) substituted barium hexaferrite nanoparticles for magnetic recording, J. Magn. Magn. Mater. 187 (1998) 129–135, http://dx.doi.org/10.1016/S0304-8853(98)00139-5.

[152] M. Sharma, S.C. Kashyap, H.C. Gupta, Effect of Mg–Zr substitution and microwave processing on magnetic properties of barium hexaferrite, Physica B 448 (2014) 24–28, http://dx.doi.org/10.1016/j.physb.2014.04.035.

[153] M.A. Almessiere, Y. Slimani, A. Baykal, Structural and magnetic properties of Ce-doped strontium hexaferrite, Ceram. Int. 44 (2018) 9000–9008, http://dx.doi.org/10.1016/j.ceramint.2018.02.101.

[154] A. Demir, S. Güner, Y. Bakis, S. Esir, A. Baykal, Magnetic and optical properties of $Mn_{1-x}Zn_xFe_2O_4$nanoparticles, J. Inorg. Organomet. Polym. Mater. 24 (2014) 729–736, http://dx.doi.org/10.1007/s10904-014-0032-1.

[155] Y. Slimani, M.A. Almessiere, S. Guner, F.S. Alahmari, G. Yasin, A.V. Trukhanov, A. Baykal, Influence of Tm–Tb substitution on magnetic and optical properties of Ba–Sr hexaferrites prepared by ultrasonic assisted citrate sol–gel approach, Mater. Chem. Phys. 253 (2020) 123324, http://dx.doi.org/10.1016/j.matchemphys.2020.123324.

[156] M.A. Almessiere, Y. Slimani, S. Guner, M. Sertkol, A. Demir Korkmaz, S.E. Shirsath, A. Baykal, Sonochemical synthesis and physical properties of $Co_{0.3}Ni_{0.5}Mn_{0.2}Eu_xFe_{2-x}O_4$ nano-spinel ferrites, Ultrason. Sonochemistry 58 (2019) 104654, http://dx.doi.org/10.1016/j.ultsonch.2019.104654.

[157] N. Boda, G. Boda, K.C.B. Naidu, M. Srinivas, K.M. Batoo, D. Ravinder, A.P. Reddy, Effect of rare earth elements on low temperature magnetic properties of Ni and Co-ferrite nanoparticles, J. Magn. Magn. Mater. 473 (2019) 228–235, http://dx.doi.org/10.1016/j.jmmm.2018.10.023.

[158] S.A. Mazen, N.I. Abu-Elsaad, A.E. Khadour, A comparative study of the structural and magnetic properties for Zn^{2+} and Ge^{4+} ions substituted nickel ferrites, J. Magn. Magn. Mater. 491 (2019) 165562, http://dx.doi.org/10.1016/j.jmmm.2019.165562.

[159] K. Al Yaqoob, M. Bououdina, M.S. Akhter, B. Al Najar, J.J. Vijaya, Selectivity and efficient Pb and Cd ions removal by magnetic MFe_2O_4 (M=Co, Ni, Cu and Zn) nanoparticles, Mater. Chem. Phys. 232 (2019) 254–264, http://dx.doi.org/10.1016/j.matchemphys.2019.04.077.

[160] C. Liu, X. Kan, F. Hu, X. Liu, S. Feng, J. Hu, W. Wang, K.M.U. Rehman, M. Shezad, C. Zhang, H. Li, S. Zhou, Q. Wu, Investigations of Ce-Zn co-substitution on crystal structure and ferrimagnetic properties of M-type strontium hexaferrites $Sr_{1-x}Ce_xFe_{12-x}Zn_xO_{19}$ compounds, J. Alloys Compd. 785 (2019) 452–459, http://dx.doi.org/10.1016/j.jallcom.2019.01.182.

[161] A. Xia, S. Ren, J. Lin, Y. Ma, C. Xu, J. Li, C. Jin, X. Liu, Magnetic properties of sintered $SrFe_{12}O_{19}$–$CoFe_2O_4$ nanocomposites with exchange coupling, J. Alloys Compd. 653 (2015) 108–116, http://dx.doi.org/10.1016/j.jallcom.2015.08.252.

[162] H. El Moussaoui, T. Mahfoud, S. Habouti, K. El Maalam, M. Ben Ali, M. Hamedoun, O. Mounkachi, R. Masrour, E.K. Hlil, A. Benyoussef, Synthesis and magnetic properties of tin spinel ferrites doped manganese, J. Magn. Magn. Mater. 405 (2016) 181–186, http://dx.doi.org/10.1016/j.jmmm.2015.12.059.

[163] B. Nandan, M.C. Bhatnagar, S.C. Kashyap, Cation distribution in nanocrystalline cobalt substituted nickel ferrites: X-ray diffraction and Raman spectroscopic investigations, J. Phys. Chem. Solids 129 (2019) 298–306, http://dx.doi.org/10.1016/j.jpcs.2019.01.017.

[164] V. Manikandan, V. Kuncser, B. Vasile, S. Kavita, S. Vigneselvan, R.S. Mane, Enhancement in magnetic and dielectric properties of the ruthenium-doped copper ferrite (Ru-$CuFe_2O_4$) nanoparticles, J. Magn. Magn. Mater. 476 (2019) 18–23, http://dx.doi.org/10.1016/j.jmmm.2018.12.050.

[165] W. Zhang, A. Sun, X. Pan, Y. Han, X. Zhao, L. Yu, Z. Zuo, N. Suo, Magnetic transformation of Zn-substituted Mg-Co ferrite nanoparticles: Hard magnetism → soft magnetism, J. Magn. Magn. Mater. 506 (2020) 166623, http://dx.doi.org/10.1016/j.jmmm.2020.166623.

[166] Y. Slimani, H. Güngüneş, M. Nawaz, A. Manikandan, H.S. El Sayed, M.A. Almessiere, H. Sözeri, S.E. Shirsath, I. Ercan, A. Baykal, Magneto-optical and microstructural properties of spinel cubic copper ferrites with Li-Al co-substitution, Ceram. Int. 44 (2018) 14242–14250, http://dx.doi.org/10.1016/j.ceramint.2018.05.028.

[167] J. Xia, X. Wu, Y. Huang, W. Wu, J. Liang, Q. Li, Enhancements of saturation magnetization and coercivity in $Ni_{0.5}Zn_{0.5}Fe_2O_4/SrFe_{12}O_{19}$ composite powders by exchange-coupling mechanism, J. Mater. Sci., Mater. Electron. 30 (2019) 11682–11693, http://dx.doi.org/10.1007/s10854-019-01527-2.

[168] M.A. Almessiere, Y. Slimani, S. Guner, S. Aldakhil, A.D. Korkmaz, M. Sertkol, H. Gungunes, G. Yasin, A. Baykal, Ultrasonic. synthesis, Ultrasonic synthesis magnetic and optical characterization of Tm^{3+} and Tb^{3+} ions co-doped barium nanohexaferrites, J. Solid State Chem. 286 (2020) 121310, http://dx.doi.org/10.1016/j.jssc.2020.121310.

[169] N. Yasmin, M. Mirza, S. Muhammad, M. Zahid, M. Ahmad, M.S. Awan, A. Muhammad, Influence of samarium substitution on the structural and magnetic properties of M-type hexagonal ferrites, J. Magn. Magn. Mater. 446 (2018) 276–281, http://dx.doi.org/10.1016/j.jmmm.2017.09.005.

[170] M.A. Almessiere, Y. Slimani, H. Gungunes, M. Sertkol, M. Nawaz, N.A. Algarou, A. Baykal, I. Ercan, Tb^{3+} substituted strontium hexaferrites: Structural, magnetic and optical investigation and cation distribution, J. Rare Earths 38 (2020) 402–410, http://dx.doi.org/10.1016/j.jre.2019.06.007.

[171] M.A. Almessiere, Y. Slimani, N.A. Tashkandi, H. Güngüneş, M. Sertkol, M. Nawaz, S. Ali, A. Baykal, I. Ercan, Tailored. microstructures, Tailored microstructures optical and magnetic qualities of strontium hexaferrites: Consequence of Tm^{3+} and Tb^{3+} Co-substitution, Ceram. Int. 45 (2019) 21385–21394, http://dx.doi.org/10.1016/j.ceramint.2019.07.126.

[172] M.A. Almessiere, Y. Slimani, S. Güner, A. Baykal, I. Ercan, Effect of dysprosium substitution on magnetic and structural properties of $NiFe_2o_4$ nanoparticles, J. Rare Earths 37 (2019) 871–878, http://dx.doi.org/10.1016/j.jre.2018.10.009.

[173] A. Xia, Y. Li, T. Li, S. Su, C. Jin, X. Liu, The availability of Henkel plots for sintered hard/soft magnetic composite ferrites, Physica B 493 (2016) 14–16, http://dx.doi.org/10.1016/j.physb.2016.04.013.

[174] M. Kahnes, R. Müller, J. Töpfer, Phase formation and magnetic properties of $CoFe_2O_4/CoFe_2$ nanocomposites, Mater. Chem. Phys. 227 (2019) 83–89, http://dx.doi.org/10.1016/j.matchemphys.2019.01.064.

[175] Y. Yang, D. Huang, F. Wang, J. Shao, An investigation on microstructural, spectral and magnetic properties of Pr–Cu double-substituted M-type Ba–Sr hexaferrites, Chinese J. Phys. 57 (2019) 250–260, http://dx.doi.org/10.1016/j.cjph.2018.11.012.

[176] S.E. Jacobo, P.G. Bercoff, C.A. Herme, L.A. Vives, Sr hexaferrite/Ni ferrite nanocomposites: Magnetic behavior and microwave absorbing properties in the X-band, Mater. Chem. Phys. 157 (2015) 124–129, http://dx.doi.org/10.1016/j.matchemphys.2015.03.026.

[177] Gang Fang, Chuyang Liu, Yun Yang, Kangsen Peng, Yufan Cao, Guoyue Xu, Yujing Zhang, High-efficiency microwave absorbing performance originating from sufficient magnetic exchange coupling interaction and impressive dielectric loss, J. Mater. Chem. C 9 (2021) 1936–1944, http://dx.doi.org/10.1039/D0TC05222A.

[178] J. Fischbacher, A. Kovacs, M. Gusenbauer, H. Oezelt, L. Exl, S. Bance, T. Schrefl, Micromagnetics of rare-earth efficient permanent magnets, J. Phys. D: Appl. Phys. 51 (2018) 193002, http://dx.doi.org/10.1088/1361-6463/aab7d1.

[179] H. Yang, T. Ye, Y. Lin, M. Liu, P. Kang, G. Zhang, Enhancements of (BH)max and remanence in $BaFe_{12}O_{19}/CaFe_2O_4/CoFe_2O_4$ nanocomposite powders by exchange-coupling mechanism, Mater. Chem. Phys. 171 (2016) 27–32, http://dx.doi.org/10.1016/j.matchemphys.2016.01.010.

[180] Gang Fang, Chuyang Liu, YunYang, Kangsen Peng, GuoyueXu, Yujing Zhang, Broad microwave absorption bandwidth achieved by exchange coupling interaction between hard and soft magnetic materials, Ceram. Int. 47 (2) (2021) 2879–2883, http://dx.doi.org/10.1016/j.ceramint.2020.09.011.

[181] A.H. Ashour, A.I. El-Batal, M.I.A.A. Maksoud, G.S. El-Sayyad, S. Labib, E. Abdeltwab, M.M. El-Okr, Antimicrobial activity of metal-substituted cobalt ferrite nanoparticles synthesized by sol–gel technique, Particuology 40 (2018) 141–151, http://dx.doi.org/10.1016/j.partic.2017.12.001.

[182] M.N. Ashiq, A.S. Asi, S. Farooq, M. Najam-ul Haq, S. Rehman, Magnetic and electrical properties of M-type nano-strontium hexaferrite prepared by sol–gel combustion method, J. Magn. Magn. Mater. 444 (2017) 426–431, http://dx.doi.org/10.1016/j.jmmm.2017.08.065.

[183] Y. Hou, F. Fan, X.-H. Wang, S.-J. Chang, Terahertz power splitter based on ferrite photonic crystal, Optik 124 (2013) 5285–5288, http://dx.doi.org/10.1016/j.ijleo.2012.06.095.

[184] Y. Wang, D. Zhang, B. Xu, Z. Dong, J. Pei, S. Xu, T-typed photonic crystal circulator with square lattice Al_2O_3 rods array and NiZn-ferrite posts, Mater. Des. 181 (2019) 107978, http://dx.doi.org/10.1016/j.matdes.2019.107978.

[185] S. Bierlich, T. Reimann, F. Gellersen, A.F. Jacob, J. Töpfer, Sintering, microwave properties, and circulator applications of textured Sc-substituted M-type ferrite thick films, J. Eur. Ceram. Soc. 39 (2019) 3077–3081, http://dx.doi.org/10.1016/j.jeurceramsoc.2019.04.014.

[186] S.R. Bhongale, Mg-Nd-Cd ferrite as substrate for X-band microstrip patch antenna, J. Magn. Magn. Mater. 499 (2020) 165918, http://dx.doi.org/10.1016/j.jmmm.2019.165918.

[187] R. Vinaykumar, J. Bera, Low-temperature sintering of $SrCo_{1.5}Ti_{1.5}Fe_9O_{19}$ ferrite and its characterization for X-band antenna application, J. Alloys Compd. 790 (2019) 413–420, http://dx.doi.org/10.1016/j.jallcom.2019.03.168.

[188] Y. Yang, J. Li, H. Zhang, G. Wang, Y. Rao, G. Gan, TiO_2 tailored low loss NiCuZn ferrite ceramics having equivalent permeability and permittivity for miniaturized antenna, J. Magn. Magn. Mater. 487 (2019) 165318, http://dx.doi.org/10.1016/j.jmmm.2019.165318.

[189] F. Xie, Y. Chen, M. Bai, P. Wang, Co-substituted LiZnTiBi ferrite with equivalent permeability and permittivity for high-frequency miniaturized antenna application, Ceram. Int. 45 (2019) 17915–17919, http://dx.doi.org/10.1016/j.ceramint.2019.06.008.

[190] S. Manjura Hoque, C. Srivastava, V. Kumar, N. Venkatesh, H.N. Das, D.K. Saha, K. Chattopadhyay, Exchange-spring mechanism of soft and hard ferrite nanocomposites, Mater. Res. Bull. 48 (2013) 2871–2877, http://dx.doi.org/10.1016/j.materresbull.2013.04.009.

[191] M. Green, X. Chen, Recent progress of nanomaterials for microwave absorption, J. Mater. 5 (2019) 503–541, http://dx.doi.org/10.1016/j.jmat.2019.07.003.

[192] A.V. Trukhanov, S.V. Trukhanov, V.G. Kostishyn, L.V. Panina, V.V. Korovushkin, V.A. Turchenko, D.A. Vinnik, E.S. Yakovenko, V.V. Zagorodnii, V.L. Launetz, V.V. Oliynyk, T.I. Zubar, D.I. Tishkevich, E.L. Trukhanova, Correlation of the atomic structure, magnetic properties and microwave characteristics in substituted hexagonal ferrites, J. Magn. Magn. Mater. 462 (2018) 127–135, http://dx.doi.org/10.1016/j.jmmm.2018.05.006.

[193] A.V. Trukhanov, V.G. Kostishyn, L.V. Panina, V.V. Korovushkin, V.A. Turchenko, P. Thakur, A. Thakur, Y. Yang, D.A. Vinnik, E.S. Yakovenko, L.Y. Matzui, E.L. Trukhanova, S.V. Trukhanov, Control of electromagnetic properties in substituted M-type hexagonal ferrites, J. Alloys Compd. 754 (2018) 247–256, http://dx.doi.org/10.1016/j.jallcom.2018.04.150.

[194] A.V. Trukhanov, K.A. Astapovich, V.A. Turchenko, M.A. Almessiere, Y. Slimani, A. Baykal, A.S.B. Sombra, D. Zhou, R.B. Jotania, C. Singh, T.I. Zubar, D.I. Tishkevich, S.V. Trukhanov, Influence of the dysprosium ions on structure, magnetic characteristics and origin of the reflection losses in the Ni–Co spinels, J. Alloys Compd. 841 (2020) 155667, http://dx.doi.org/10.1016/j.jallcom.2020.155667.

[195] C.G. Koops, On the dispersion of resistivity and dielectric constant of some semiconductors at audiofrequencies, Phys. Rev. 83 (1951) 121–124, http://dx.doi.org/10.1103/PhysRev.83.121.

[196] L.G. Van Uitert, Dielectric properties of and conductivity in ferrites, Proc. IRE 44 (1956) 1294–1303.

[197] L.G. Van Uitert, High-resistivity nickel ferrites — the effect of minor additions of manganese or cobalt, J. Chem. Phys. 24 (1956) 306–310, http://dx.doi.org/10.1063/1.1742468.

[198] R. Parker, B.A. Griffiths, D. Elwell, The effect of cobalt substitution on electrical conduction in nickel ferrite, Br, J. Appl. Phys. 17 (1966) 1269–1276, http://dx.doi.org/10.1088/0508-3443/17/10/303.

[199] T. Maeda, S. Sugimoto, T. Kagotani, N. Tezuka, K. Inomata, Effect of the soft/hard exchange interaction on natural resonance frequency and electromagnetic wave absorption of the rare earth–iron–boron compounds, J. Magn. Magn. Mater. 281 (2004) 195–205, http://dx.doi.org/10.1016/j.jmmm.2004.04.105.

[200] V. Nandwana, R. Zhou, J. Mohapatra, S. Kim, P.V. Prasad, J.P. Liu, V.P. Dravid, Exchange coupling in soft magnetic nanostructures and its direct effect on their theranostic properties, ACS Appl. Mater. Interfaces 10 (2018) 27233–27243, http://dx.doi.org/10.1021/acsami.8b09346.

[201] C. Feng, X. Liu, S.W. Or, S.L. Ho, Exchange coupling and microwave absorption in core/shell-structured hard/soft ferrite-based $CoFe_2O_4/NiFe_2O_4$ nanocapsules, AIP Adv. 7 (2016) 56403, http://dx.doi.org/10.1063/1.4972805.

[202] S. Hazra, N. Ghosh, Preparation of nanoferrites and their applications, J. Nanosci. Nanotechnol. 14 (2014) 1983–2000, http://dx.doi.org/10.1166/jnn.2014.8745.

[203] S. Tyagi, P. Verma, H.B. Baskey, R.C. Agarwala, V. Agarwala, T.C. Shami, Microwave absorption study of carbon nano tubes dispersed hard/soft ferrite nanocomposite, Ceram. Int. 34 (2012) 4561–4571, http://dx.doi.org/10.1016/j.ceramint.2012.02.034.

[204] X.Q. Shen, F.Z. Song, J. Xiang, M.Q. Liu, Y.W. Zhu, Y.D. Wang, Shape anisotropy, Shape anisotropy exchange-coupling interaction and microwave absorption of hard/soft nanocomposite ferrite, J. Am. Ceram. Soc. 95 (2012) 3863–3870, http://dx.doi.org/10.1111/j.1551-2916.2012.05375.x.

[205] Y. Wang, Y. Huang, Q.F. Wang, Preparation, and magnetic properties of $BaFe_{12}O_{19}/Ni_{0.8}Zn_{0.2}Fe_2O_4$ nanocomposite ferrite, J. Magn. Magn. Mater. 324 (2012) 3024e3028, http://dx.doi.org/10.1016/j.jmmm.2012.04.059.

[206] K.W. Moon, S.G. Cho, Y.H. Choa, K.H. Kim, J. Kim, Synthesis and magnetic properties of nano Ba-hexaferrite/NiZn ferrite composites, Phys. Status Solidi (a) 204 (12) (2007) 4141, http://dx.doi.org/10.1002/pssa.200777228.

[207] M. Kahnes, J. Töpfer, Synthesis and magnetic properties of hard/soft $SrAl_2Fe_{10}O_{19}/Fe(FeCo_2)$ nanocomposites, J. Magn. Magn. Mater. 480 (2019) 40–46, http://dx.doi.org/10.1016/j.jmmm.2019.02.065.

[208] A. Hernando, J. González, Soft and hard nanostructured magnetic materials, Hyperfine Interact. 130 (2000) 221–240, http://dx.doi.org/10.1023/A:1011096522429.

[209] J. Arcas, A. Hernando, J. Barandiarán, C. Prados, M. Vázquez, P. Marín, A. Neuweiler, Soft to hard magnetic anisotropy in nanostructured magnets, Phys. Rev. B 58 (1998) 5193, http://dx.doi.org/10.1103/PhysRevB.58.5193.

[210] X. Liu, W. Zhong, B. Gu, Y. Du, Exchange-coupling interaction in nanocomposite $SrFe_{12}O_{19}$/gamma-Fe_2O_3 permanent ferrites, J. Appl. Phys. 92 (2002) 1028–1032, http://dx.doi.org/10.1063/1.1487908.

[211] C. Pahwa, S. Mahadevan, S. Bindr, Narang, P. Sharma, Structural, magnetic and microwave properties of exchange coupled and non-exchange coupled $BaFe_{12}O_{19}/NiFe_2O_4$ nanocomposites, J. Alloys Compd. 725 (2017) 1175–1181, http://dx.doi.org/10.1016/j.jallcom.2017.07.220.

[212] S. Hazra, B.K. Ghosh, H.R. Joshi, M.K. Patra, R.K. Jani, S.R. Vadera, N.N. Ghosh, Development of a novel one-pot synthetic method for the preparation of $(Mn_{0.2}Ni_{0.4}Zn_{0.4}Fe_2O_4)_x$–$(BaFe_{12}O_{19})_{1-x}$ nanocomposites and the study of their microwave absorption and magnetic properties, RSC Adv. 4 (2014) 45715–45725, http://dx.doi.org/10.1039/C4RA07145J.